Subj.: Re-submission of manuscript nhess-2017-111

Dear Paolo Tarolli,

This cover letter is to go with our electronic re-submission of the manuscript *Criteria for the optimal selection of remote sensing images to map event landslides* by Federica Fiorucci, Daniele Giordan, Michele Santangelo, Furio Dutto, Mauro Rossi, Fausto Guzzetti.

We are grateful to you and to the two reviewers for their constructive comments that helped us to improve the work.

In preparing the new version of our work, we considered all the comments and suggestions made by the two referees, which were pertinent and helpful.

To respond to the requests of both the reviewers we modified the Title, and all the other sections according to the reviewer requests. We added three new figures as requested by the reviewers.

We provide a list of our responses to the referee's comments, including details on the changes made to the text.

Overall, we consider this new version of the manuscript significantly improved. We hope the paper can be accepted for publication in the Special Issues: *The use of remotely piloted aircraft systems (RPAS) in monitoring applications and management of natural hazards*.

We look forward to hearing a decision from you soon.

Sincerely,
Federica Fiorucci, on behalf

Answer to referee # 1

The authors present a study focussing on an expert-based interpretation of imagery data with the aim of mapping landslide features of a single landslide. Various data are tested and the mapping results are compared to reference data and field mappings.

The authors then give recommendations regarding the feasibility of the different mapping techniques and imagery data for landslide mapping. The employed methods are standard methods (dGPS, heuristic landslide mapping techniques), so there is no methodical innovation. The used software are commercial products. The results are difficult to reproduce, since only one expert did all the mapping. It would be interesting to see, how the landslide would have been mapped by further experts (>10). Furthermore, it remains unclear if the results are transferable to the relevant scale of event landslide inventories or to other types of landslides.

We thank this Reviewer (R1) for this comment. As correctly noted by R1, in this work we adopted different (standard) techniques and digital images to produce a landslide inventory. The techniques consist in field mapping and photointerpretation. For the latter we used six different digital products. However, we point out that the aim of the effort was not to investigate the feasibility of techniques, nor to give absolute criteria to choose among different images. The study focuses on the definition of criteria for the selection of remote sensing images for the specific purpose of mapping event landslides. For this reason, we relied upon a single expert to perform the landslide recognition and mapping. We considered the possibility to use more experts. However, this would have added the uncertainty inherent in the subjective interpretation of aerial photography for landslide mapping (see e.g., Carrara et al., 1992, Uncertainty in evaluating landslide hazard and risk. ITC Journal, 172–183). The uncertainty inherent with the interpreters would have mixed (and covered partially) the "signal" from the different imagery used for our experiment. Since the scope of the research was to investigate the information content of the imagery (and not of the interpreters) we ruled out the possibility of using more interpreters. Further, the researcher geomorphologist who interpreted the images and prepared the maps (MS) has a significant experience in photointerpretation for landslide mapping (he has prepared 25 landslides maps, including event maps, geomorphological maps, multi-temporal maps, covering more than 4000 km^2, obtained using both monoscopic and stereoscopic satellite images and stereoscopic aerial photographs). Thanks to the expertise of the mapper, in each digital image the relevant features of the landslide were recognized fully. Thus, we are confident that differences among the six maps are to be ascribed to the sole resolving power of the different images. We have clarified this point in the text (see below). Moreover, we selected a landslide having both morphological and photographical signatures, which are the two key features that allows to recognize and map landslides from digital images. For this reason, we maintain that the results we have obtained are valid at all scales, and for most landslide types.

The text is generally well written, but there are some minor mistakes of grammar and style. Some of them are addressed below, but it would be out of scope to raise every issue. Therefore, I recommend careful copy editing. Below, I focus on issues concerning the scientific content of the manuscript. Where numbers are given in the specific comments *they refer to the manuscript page and line. A major revision carefully addressing the raised issues below is required, before the paper can be considered for publication.*

We thank R1 for reading carefully or Manuscript. We amended the text following R1 suggestions, where applicable.

Specific Comments

Consider introducing the principle of heuristic, visual mapping of landslide features based on the interpretation of landslide signs ('geometric signature'; Pike, 1988). This is well explained in Section 4.2. However, an introductory description of the procedure would benefit the understanding of the reader. In this context, also explain the advantage of stereoscopic over monoscopic interpretation techniques.

In the Introduction, we added the following language to clarify the text:

"The heuristic visual mapping of landslide features is based on the systematic analysis of image photographic and morphological characteristics such as colour, tone, mottling, texture, shape, size, curvature (Pike 1988). These photographic and morphological characteristics encompasses all the possible landslide features that can be used for the (visual) interpretation of the available imagery."

Consider addressing the necessary positional accuracy of the mapped landslide features with respect to the intended use/scale of the compiled landslide inventory.

We accepted this suggestion of R1. In the Discussion section, we added the following sentence:

"Where possible, we recommend that the acquisition of images used for the production of event, seasonal or multi-temporal landslide inventory maps is planned considering the typical landslide signature, in addition to the purpose (event inventory, planning of monitoring systems), scale of the mapping (i.e. regional or slope scale), and the size and complexity of the study area (see Table 3)."

Consider adding a sentence addressing the potential of UAV-based imagery for efficiently analysing changes over time (e.g. Turner et al., 2015). Added to Discussion section.

We accepted this suggestion of R1. In the Discussion, we added the following sentence:

"The use of UAV images was recently proposed by Turner et al. (2015) for determining the landslide dynamics, exploiting time series of images that can be constructed using UAVs. The result is achievable thanks to centimetre co-registration accuracy of the UAV images."

Which type of landslide is it, what type of material is involved (since the area seems to be not very steep) and what are the causes and failure mechanism?

We accepted the comment of R1, and changed the text as follows:

“For our study, we selected the Assignano landslide, a slide-earthflow (Hutchinson, 1970) triggered by intense rainfall in December 2013 in the northwest-facing slope of the Assignano village, Umbria, central Italy (Fig. 1). The landslide develops in a crop area, where a layered sequence of sand, silt and clay deposits crop out (Santangelo et al., 2015)”.

Have there been changes during the winter months (e.g. retrogressive failure, erosion)?

For the purposes of the present study this information is not relevant. No changes were recorded between the field mapping and the time of the acquisition of the images. However, after the mapping procedure was completed, a retrogressive movement occurred in the landslide escarpment area. This is visible on the recent images provided by Google Earth.

Is the area cultivated/what is the land cover/land use?

To respond to the question of R1, we modified the text adding the following sentence:

“The landslide develops in a crop area, and the lithology consists in a sequence of sand, silt and clay layered deposits.”

Add a table specifying what was done by whom and when. Also include the abbreviations of the persons.

We considered carefully the option of adding a table, as suggested by R1. However, we concluded that this was not necessary, and would only add to the length of the paper, without improving clarity or readability. The abbreviation of the individuals who performed the GPS mapping and photointerpretation are given in sections 4.1 and 4.2.

Describe the 2.5D pseudo-stereoscopic data in more detail. Why was the landslide mapping based on the orthorectified UAV-imagery done in Google Earth and not using a more suited GIS software?

We acknowledge that our choice us using Google Earth™ was poorly explained. We have changed and expanded the text, that now reads:

“To interpret visually the ultra-resolution UAV image, the interpreter overlaid (“draped”) the image on Google Earth™. For the purpose, we first treated the UAV image with the gdal2tiles.py software to obtain a set of image tiles compatible with Google Earth™ terrain visualization platform. To the best of our knowledge, the platform is the only free, 2.5D image visualisation environment that allows the editing of vector (i.e., point, line, polygon) information. Other commercial (e.g., ArcScene) and open source (e.g., ParaView, GRASS GIS), 2.5D visualization tools do not provide editing capabilities. Google Earth™ is a user-friendly solution for mapping single landslides, and for preparing landslide event inventories for limited areas, with the possibility for the user to visualize a landscape from virtually any viewpoint, facilitating landslide mapping”.

Did you use the DEM included in Google Earth for aiding the mapping procedure?

The DEM available in Google Earth™ is low-resolution, pre-event DEM, that does not provide adequate information on the specific landslide morphology. On the other hand, the DEM proves useful to frame the landslide in the general morphology of the slope.

Why didn't you consider a DEM based on the UAV-point cloud?

Indeed, we considered this option carefully. However, to the best of our knowledge, there is no dedicated 2.5D GIS software that allows for editing on a custom DEM used to drape ortho-photographs. The only way to use the DEM based on the UAV-point cloud would have been to use a dedicated GIS for 2.5D visualization software, and a 2D GIS editing environment to transfer the information obtained from the visualization to a base map. The procedure would have introduced an additional source of uncertainty.

Since in most of the scene there is no high vegetation (trees), the landslide's morphology should be represented well. Also other derivatives of the resulting UAVC3 NHESSD Interactive Comment Printer-friendly version Discussion paper based DEM (e.g. shaded reliefs, e.g. Niethammer et al., 2010) could be used for landslide mapping. Then, also the morphometric features could have been mapped better using the UAV data.

The use of maps derived from the elevation data is out of the scope of the work, and of the paper that focuses on optical images. We acknowledge that the scope of the work was not fully clear. When have changed the tithe that now reads "Criteria for the optimal selection of remote sensing optical images to map event landslides". We also added the word "optical" in the Introduction, where we now write:

"These maps were compared to an eighth map considered to be the benchmark showing the "ground truth" i.e., the "true" position, shape and extent of the Assignano landslide. Based on the results of the map comparison, we infer the ability of different optical images, characterized by with different spectral and spatial characteristics, to portray the landslide features that can be exploited for the visual detection and mapping of landslides."

Describe the transfer of mapped landslide features from Google Earth to the GIS. Which GIS software was used?

To transfer the mapped landslide features from Google Earth™ to a GIS database we used the open source GIS software QGIS. The mapping produded in Google Earth™ was imported in QGIS as a Keyhole Markup Language (kml) file, and then converted in the ESRI Shapefile (shp) format.

Which coordinate system/projection was used for the individual datasets (can Google Earth handle ETRF-2000)?

Seven of the dataset were originally mapped in WGS 84 33 N (EPSG 32633). Concerning the question about the capacity of Google Earth to handle ETRF-2000 reference system, we acknowledge that some errors are expected when a raster map is warped on Google Earth, due primarily to the spherical Mercator reference system adopted by Google Earth). However, we did not observe relevant systematic positional errors. This is evident also when comparing the map obtained using the monoscopic UAV image with the map obtained overlaying ("draping") the same image on Google Earth™.

Mention that you mapped the source/transportation area and the deposition area as separate landslide features. How did you discern the source/transportation area from the deposition area?

To respond to this comment of R1, we added language to the paragraph. The new text now reads:

"The source and transportation area is bounded locally by sub-vertical, 2 to 4-m high escarpments. In the landslide, terrain slope averages 11°, and is steeper (12°) in the source and transportation area than in the deposition area (9°). The landslide signature (Pike, 1988) is different in the different parts of the landslide. In the source and transport area the signature is predominantly photographical (radiometric), whereas in the landslide deposit it is mainly morphometric (topographic). The differences allow to separate the source and transportation area from the deposition area".

Are there indicators beyond subjective visual recognition?

We are not sure we understand fully the question. However, we point out that visual recognition is by definition subjective, but it is based on objective and reproducible observations. As stated in section 2, the two landslide portions show different average slope and different photographical and morphological signatures. An expert geomorphologist is able to identify and classify the different landslide signatures, in the source and transport zone and in the deposition area.

How did you treat shadows during landslide mapping?

The images we used were free from shadows.
We added language in Section 3 to state that:

"Both satellite and UAV images are free from deep shadows (**Fig. 2**)."

Comment on the comparability of landslide features mapped on different scales (1:1.000 to 1:6.000).

We accepted this comment of R1, and we changed the text adding the following sentence to paragraph 4.2:

"The scale of observation was selected to obtain the best readability of each landslide feature and the surroundings, which is a common practice in image visual analysis for landslide mapping (Fiorucci et al., 2011). Hence, even if the maps were produced at slightly different observation scales, the differences arising from the comparison are due to actual features (i.e., the image resolution and radiometry), and not to the different observation scales."

Technical comments

We thank R1 for the technical comments. We accepted all the technical comments of R1, and we corrected the text accordingly.

Figures and Tables

Figure 1: add information on the shown datasets in Fig. 1A (also add a reference to Google Earth), also specifying the source of the polygons and -lines.

To respond to this request of R1, we added language in the caption, that now reads:

"The Assignano landslide, located near Collazzone, Umbria, central Italy. (A) global view of the landslide. (B) detail of the landslide source area. (C) detail of the landslide transportation area. (D) detail of the landslide deposit. Base image obtained overlaying ("draping") the image on Google Earth™. Red line is the boundary of the landslide obtained using the RTK DGPS (benchmark)".

Figure 2: Add a north arrow. Change DGPC to DGPS in the caption.

In the new version of the manuscript Figure 2 has become Figure 5. We thank R1 for the suggestion, and we change the figure and the caption accordingly.

Table 1: change meter to metre in the caption

We accepted this suggestion of R1, and amended the caption accordingly.

Reference

We added to the list of references the three citations suggested by R1.

Answer to referee # 2

This paper aims at comparing different geological mapping of the perimeter of an Italian landslide within a temperate area partially covered with forested vegetation. The authors realize that high resolution, various wave length and stereoscopic views helps a lot in order to precise the external geometry of some sections of this landslide (crown transport and sedimentation areas). Moreover, authors quantify the misfit in between those different mappings relative to a benchmark (Field RTK DGPS survey) through a useful error matrix. The differences in the mapping partly derived from the forest cover that hide the exact perimeter of this landslide.

To my point of view, the main teaching of this paper is not new as geologists/geomorphologists experts in mapping know since a long time that very high resolution, as well as False color composition (relative to True color) and stereoscopic analyses are major and compulsory keys for a precise and exact geological/geomorphological mapping of any geological/geomorpholoigcal objects. Moreover, planimetric differences of mapped objects also are not new see for instance the work on various fractal distances on the measurements of a Britany shoreline that change a lot function of the scale and the resolution (see the basic work of the mathematician benoit Mandelbrot ENSMP Fontainebleau and his team in the 1980's). The interest of this paper is to illustrate it correctly with a pedagogic example and to recall to any scientists these facts using a specific example. In that sense it is interesting for NHESS to publish it.

We thank this Reviewer (R2) for this comment. R2 is correct in saying that our work (and the paper) article does not introduce novelty concerning the adopted techniques used to recognize and map landslides. Indeed, the purpose of the work is to identify which images characteristics are more suitable to map landslide features. With this respect, and to the best of our knowledge, we maintain that there are not very many examples in the landslide literature. Mapping differences are not related to the presence of vegetation (we are working in a crop area and not in forested terrain), but rather to the ability of the images to highlight the two key landslide features, namely: the morphological and photographical signatures. Moreover, we show that the highest resolution or the FCC may not be the best choice for landslide recognition and mapping. Since landslide features are predominantly morphological, this work shows that it can be preferable to use stereoscopic images with smaller spatial resolution than ultra-resolution monoscopic images.

Could you differentiate more clearly the 3 sections of this landslide on those various mapping erosional part (crown), transport section, and at least the sedimentational section (toe). With which image (and why) do we have the best and the more exact geological mapping of this landslide?

The best (and "more exact") landslide mapping could be considered the one obtained using stereoscopic satellite TC image for the deposition area (E = 0.21) and the monoscopic UAV image for the source and transportation area (E = 0.15). Overall, and considering the entire landslide, the best mapping (i.e., the one most similar to the benchmark) is the one obtained using Stereoscopic Satellite TC image (E = 0.18). The mentioned numerical values of the error (Error Index proposed by Carrara et al., 1992) are shown in Figure 6. Concerning the choice of a single "best" image, the issue is discussed in the last paragraphs of the "Concluding remarks". The discussion is done from a wider point of view than the investigation of the specific landslide considered in this work. In fact, we conclude that the choice of the best type of image is dictated by technical and cost-related constraints. We stress that this work focuses on the identification of the characteristics of the images that enable the best recognition and mapping of landslide features. Distinguishing between the different kinematic domains of the landslide, or recognizing geological or geotechnical features of the landslide, is out of the scope of this research wor

Could you precise the inputs and differences through local case examples on a new figure of high resolution DTM, FCC and stereoscopic mapping in order that the reader will be able to get an independent position.

To respond to this comment of R2, we added a new figure (Figure 2). In this Figure we show the WorldView-2 images in TC and FCC, and the UAV image. For each image, we also show a detail of the source and of the deposition area. We decided against adding a stereoscopic image, mainly because a printed anaglyph does not provide the same information of a digital stereoscopic system, that is the one used by the geomorphologist to produce the maps. As such, the anaglyph would have provided potentially misleading information. Lastly, we did not use the high-resolution DEM to prepare the landslide maps.

Please finally dealing with your experience on that landslide what (and why) is your best and more exact mapping? please justify it?

We maintain we have already answered to this question of R2.

What is your best methodological solution to map precisely such Italian landslides?

The Assignano landslide represents an instructive, didactic example of a landslide that has both clear photographical and morphological signatures. By using different images, with different spectral and spatial characteristics, and comparing the maps obtained to a defined benchmark, the more accurate and cost-effective mapping is the one obtained by using the UAV image heuristic interpretation method. This is clearly the case if one considers the mapping of just one landslide. We stress that selecting the best mapping of the Assignano landslide is not the goal of this work, as clearly stated in the "Concluding remarks", and specifically in the last paragraph, where we write:

"Although we conducted our study on a single landslide (Fig. 1), we maintain that the findings are general, and can be useful to decide on the optimal imagery and technique to be used when planning the production of a landslide inventory map."

To further clarify the issue, in the revised version of the manuscript, we added the following sentence in the Introduction:

"We maintain that the results obtained in our test case are general, and should be considered for the optimal selection of images for the detection and mapping event landslides.".

If you compare the benchmark and the mappings the map E (stereoscopic image seems the best fit... could you comment on that?

A comparison between the different mappings and the benchmark are shown in Figure 5 and quantified, using the Error Index *E*, in Figure 6-III. The smallest *E* value corresponds to Map E. This means that the stereoscopic satellite image with true colours has the characteristics to resolve the photographical and morphological signature of the landslide. Thus, for our test case, it is the best image. When the morphological and photographical features are investigated separately, the best choice is Map E for the morphological features, and Map G for the photographical features, as shown in Figure 6-II and Figure 6-I, respectively.

Definitely I do not understand the misfit between map A (field DGPS survey) and map B (field landslide mapping), could you comment on the expert's landslide mapping discrepancies?

The field mapping activities consisted in (i) a reconnaissance field survey and (ii) in RTK GPS aided survey are described in detail in Section 4.1. The two mapping methods have inherently different levels of accuracy. The reconnaissance field survey is a multi-step, manual procedure, whereas the RTK GPS aided survey consists in an automatic measurement, with a well-defined accuracy dictated by the D-GPS technology of about 2 to 5 centimeters. The explanation is given in Section 4.1.

into details:

p4. line92-94: precise ...predominantly photogrammetric... and morphometric...

The signature of a landslide is photographical and not photogrammetric. For photographic signature we intend that the landslide is recognizable on the images thanks to photographic characteristic of the image, including tone, colour, tone, mottling, and texture. We change the word “morphometric” with the word “morphological”.

p5. line 108: an horizontal...

We do not accept this editorial suggestion of R2. This is because the “h” of “horizontal” is pronounced as an aspirate.

page 6, line 162: field

We thank R2 for this suggestion. We corrected the error accordingly.

page7 line 182: perform an heuristic

As before, do not accept this editorial suggestion of R2. This is because the “h” of “horizontal” is pronounced as an aspirate.

page 8, l221: this source area was characterized by small cracks (please show on a figure those features.

To respond to this request of R2, we have added the new Figure 2.

page 9, line 228 to 257 the comments of the table 2 is difficult to follow could you find an easier solution more convenient and easier to understand to present those results?

We maintain that providing (e.g., in Table 2) and describing landslide key and standard measures is useful. For this reason, we have not changed this part of the text.

P.11 , line 282 poor agreement please precise...

We acknowledge the problem, and we chanced the text. In the attempt to clarify the meaning, we now use “high value of the error index” instead of “poor agreement”.

P.11, line 287: good agreement please precise...

We acknowledge the problem, and we chanced the text. In the attempt to clarify the meaning, we now use “low value of the error index” instead of “good agreement”.

P.13, line 343 please precise a sentence on the resolution of the NIR datasets used herein and what could be the inputs if the NIR dataset if it would have 3x3cm^2 ground resolution...

To respond to this comment of R2, we added the following sentence:

“We conclude that use of the additional information contributed by the Near Infrared (NIR) band in the 1.84-m resolution satellite image did not improve the quality of the mapping. On the other hand, the contribution of the NIR in the 3-cm UAV image remains unknown.”

P.14 line 385 ...is comparable...is to my point of view poor... We do need to have precision on the differences in between mapping from stereoscopic and high resolution... You are working on a local case example you should go farther on your reflection and give to the scientific community your choice of the best way to map such kind of landslide.

The comparison among the different maps obtained using stereoscopic satellite images and UAV images is supported by the value of the error index E, which is $0.20 \geq E \geq 0.26$ for the entire landslide, $0.21 \geq E \geq 0.29$ for the deposition area, and $0.20 \geq E \geq 0.25$ for the transportation area. The mentioned E values are given in the manuscript, and our conclusions are unambiguously drawn on the basis of the analysis of such values. In particular, the main difference between maps obtained from stereoscopic and UAV images is in the mapping of the deposition area, where the morphological signature of the landslide was better detected using the stereoscopic satellite image than using the ultra-resolution monoscopic images ($0.21 \geq E \geq 0.29$). This is also stated in the “Concluding remarks”. We maintain that the selected test case is well representative of the scenarios one may be presented with in the visual mapping of a earthlow.

P.14, lines 396-397: and partly independent from the local lighting conditions including the cloud cover... please precise...

The acquisition of an UAV image can be planned selecting the best light conditions. This because, most commonly, is the UAV operator that decides when to fly. Also, the flight altitude of a UAV is typically much lower than the clouds height.

p.15, l 407 flying

We thank R2 for picking up the error. We amended the text accordingly.

P.15, l. 412: large or very large areas...

To respond to this comment of R2, we modified the text as follow:

"Fourth, a comparative analysis of the technological constrains and the costs of acquisition and processing of ultra-resolution imagery taken by UAV, and of high, or very-high resolution imagery taken by optical satellites, revealed that the ultra-resolution images are well suited to map single event landslides, clusters of landslides in a single slope, or a few landslides in nearby slopes in a small area (up to few square kilometres, Giordan et al., 2017) , and prove unsuited to cover large and very large areas where the stereoscopic satellite images provide the most effective option (Boccardo et al., 2015)".

p.16, l 447-448: a better resolution and spectral resolution did not contribute significantly to reducing the mapping errors: ??? please precise...

R2 is right in saying that the highest resolution images did not provide the best result for the purpose of this work and for the test case. This is mainly due to the fact that resolution is not the only characteristic of a remotely-sensed image. Other characteristics relevant to landslide recognition and mapping are the stereoscopic view and the spectral content. The outcome of this work shows that stereoscopic view is a key requirement to accurately recognize and map landslide features. In the depositional area, the lowest error is obtained using the stereoscopic satellite images. Even if the UAV images have a spatial resolution higher than the satellite images, the mapping error in the depositional area remains larger than the error obtained using the stereoscopic satellite images. On the other hand, the comparison between the mapping obtained from the stereoscopic satellite images in TC and stereo satellite images in FCC, don't highlight differences, meaning that to map depositional area with mainly morphological signature, stereoscopy is the most important characteristic. To clarify the issue, we added the following sentence:

"FCC and TC in the stereoscopic satellite images give similar values of the error. This indicates that the spectral resolution of the images does not provide useful information to recognize and map the landslide morphological features. On the other hand, the high spatial resolution provided by the UAV images reduces the error, when compared to the monoscopic satellite imagery. However, the error obtained using the UAV images remains higher than that obtained using stereoscopic satellite images, despite the latter having a pixel one order of magnitude larger than the UAV images. We conclude that the increase in the spatial resolution improves the ability to map morphological features when using monoscopic images.

p.16, l 461: *prove to be very effective*

We thank R2 for the suggestion, and we amended the sentence accordingly.

P. 17, 8 l 481 acknowledgments the references needs to be carefully checked.

We checked the acknowledgments the list of references.

Fig.1 to 4: please give comments within the legend that give the key points of the figures.

We changed the captions of Figures 4, 5 are 6 accordingly, to give to the reader a key point of the figure.

Figure 4. We add in the caption the following sentence:

“The photographs taken in the field and the Google Earth™ image were used to prepare the reconnaissance field map.”

Figure 5. We added the following sentence to the caption:

“Visual inspection of the images reveals the maps most similar to the benchmark.”

Figure 6. We added the following sentences to the caption:

“The error index (*E*) proposed by Carrara et al. (1992), was used to compare quantitatively the different landslide maps.”

“E spans the range from 0 (perfect matching) to 1 (complete mismatch).”

Add a figure with specific details inputs of the landslide and compare it to the different geological mappings.

We have added the new Figure 2 to show the WorldView-2 images in TC and FCC, and the UAV image. For each image details of the landslide source and depositional areas are also shown.

Criteria for the optimal selection of remote sensing optical images to map event landslides

Fiorucci F.[1], Giordan D.[2], Santangelo M.[1], Dutto F.[3], Rossi M.[1], Guzzetti F.[1]

1 Istituto di Ricerca per la Protezione Idrogeologica, Consiglio Nazionale delle Ricerche, via della Madonna Alta 126, 06128 Perugia, Italy

2 Istituto di Ricerca per la Protezione Idrogeologica, Consiglio Nazionale delle Ricerche, Strada delle Cacce 73, 10135 Torino, Italy

3 Servizio Protezione Civile della Città Metropolitana di Torino, Via Alberto Sordi 13, 10095 Grugliasco, Italy

Correspondence to: Federica Fiorucci (Federica.Fiorucci@irpi.cnr.it)

Abstract

We executed an experiment to determine the effects of optical image characteristics on event landslide mapping. In the experiment, we compared eight maps of the same landslide, the Assignano landslide, in Umbria, ~~central~~Central Italy. Six maps were obtained through the expert visual interpretation of monoscopic and pseudo-stereoscopic (2.5D), ultra-resolution (3 × 3 cm) images taken on 14 April 2014 by a Canon EOS M photographic camera flown by an CarbonCore 950 hexacopter over the landslide, and of monoscopic and stereoscopic, true-colour and false-colour-composite, 1.84 × 1.84 m resolution images taken by the WorldView-2 satellite also on 14 April 2014. The seventh map was prepared through a reconnaissance field survey aided by a pre-event satellite image taken on 8 July 2013, available on ~~Goggle~~Google Earth™, and by colour photographs taken in the field with a hand-held camera. The images were interpreted visually by an expert geomorphologist using the StereoMirror™ hardware technology combined with the ERDAS IMAGINE® and Leica Photogrammetry Suite (LPS) software. The eighth map, which we considered our reference showing the "ground truth", was obtained through a Real Time Kinematic ~~differential GPS~~Differential Global Positioning System (GPS) survey conducted by walking a GPS receiver along the landslide perimeter to capture geographic coordinates every about 5 m, with centimetre accuracy. The eight maps of the Assignano landslide were stored in a Geographic Information System (GIS~~,~~), and compared adopting a pairwise approach. Results of the comparisons, quantified by the error index E, revealed that where the landslide signature was primarily photographical (in the landslide source and transport area) the best mapping results were obtained using the higher resolution images, and where the landslide signature was mainly morphometric (in the landslide deposit) the best results were obtained using the stereoscopic images. The ultra-resolution image proved very effective to map the landslide, with results comparable to those obtained using the stereoscopic satellite image. Conversely, the field-based reconnaissance mapping provided the poorest results, measured by large mapping errors, and confirmed the difficulty in preparing accurate landslide maps in the field. Albeit conducted on a single landslide, we maintain that our results are general, and provide useful information to decide on the optimal imagery for the production of event, seasonal and multi-temporal landslide inventory maps.

1 Introduction

Accurate detection of single landslides has different scopes, including landslide mapping (Di Maio and Vassallo, 2011; Manconi et al., 2014; Plank et al., 2016), landslide hazard analysis and risk assessment (Allasia et al., 2013), to support the installation of landslide monitoring systems (Tarchi et al., 2003; Teza et al., 2007; Monserrat and Crosetto, 2008; Giordan et al., 2013), and for landslide geotechnical characterization and modelling (Gokceoglu, 2005; Rosi et al., 2013). Mapping of single landslides can be executed using the same techniques and tools commonly used by geomorphologists to prepare landslide inventory maps i.e., ~~thought~~through field surveys (Santangelo et al., 2010) or the heuristic visual interpretation of monoscopic or stereoscopic aerial or satellite images (Brardinoni et al., 2003; Fiorucci et al., 2011; Ardizzone et al., 2013), of LiDAR-derived images (Ardizzone et al., 2007; Van Den Eeckhaut et al., 2007; Haneberg et al., 2009; Giordan et al., 2013; Razak et al., 2013; Niculita et al., 2016, Petschko et al., 2016), or of ultra-resolution images acquired by Unmanned Aerial Vehicles (UAV, Niethammer et al., 2010, Giordan et al., 2015a, 2015b; Torrero et al., 2015~~). ~~, Turner et al., 2015). The heuristic visual mapping of landslide features is based on the systematic analysis of image photographic and morphological characteristics such as colour, tone, mottling, texture, shape, size, curvature (Pike, 1988). These photographic and morphological characteristics encompasses all the possible landslide features that can be used for the (visual) interpretation of the available imagery.

All these mapping techniques have inherent advantages and intrinsic limitations, which depend on the size and type of the landslides, and on the characteristics of the images, including their spatial and spectral resolutions (Fiorucci et al., 2011). As a result, landslide maps prepared exploiting one or more of the mentioned techniques are inevitably incomplete, and contain errors in terms of the position, size~~,~~ and shape of the mapped landslides (Guzzetti et al., 2000; Galli et al., 2008, Santangelo et al., ~~2015~~2015a).

Attempts have been made to evaluate the errors associated to different types of landslide inventory maps (Carrara et al., 1992; Ardizzone et al., 2002, 2007; Van Den Eeckhaut et al., 2007; Fiorucci et al., 2011; Santangelo et al., 2010; Mondini et al., 2013). Most of these attempts compare landslide maps prepared using aerial or satellite images to maps obtained through reconnaissance field mapping (Ardizzone et al., 2007; Fiorucci et al., 2011) or GPS surveys (Santangelo et al., 2010). Conversely, only a few authors have attempted to evaluate the influence of different types of imagery on landslide detection and mapping (Carrara et al., 1992).

In this work, we evaluate how images of different ~~type~~types and characteristics influence event landslide mapping. We do this by comparing eight maps of a single, rainfall-induced landslide near the village of Assignano, Umbria, central Italy. Seven maps of the same landslide were obtained using different techniques and images, including (i) a reconnaissance field survey, (ii) the interpretation of ultra-resolution images taken by an optical camera on-board an UAV, and (iii) the visual interpretation of ~~VHR,~~Very High Resolution (VHR), monoscopic and stereoscopic, multispectral images taken by the WordView-2 satellite. These maps were compared to an eighth map considered to be the benchmark showing the "ground truth" i.e., the "true" position, shape and extent of the Assignano landslide. Based on the results of the map~~-~~ comparison, we infer the ability of different optical images, ~~characterized by~~with different spectral and spatial characteristics, to portray the landslide features that can be exploited for the visual detection and mapping of landslides. We maintain that the results obtained in our test case are general, and should be considered for the optimal selection of images for the detection and mapping event landslides.

2 The Assignano landslide

For our study, we selected the Assignano landslide~~ that was~~, a slide-earthflow (Hutchinson, 1970) triggered by intense rainfall in December 2013 in the northwest-facing slope of the Assignano village, Umbria, central Italy (**Fig.** ~~1). The landslide~~ **1**). The landslide develops in a crop area, where a layered sequence of sand, silt and clay deposits crop out (Santangelo et al., 2015b). The slope failure is about 340 m long, 40 m wide in the transportation area, and 60 m wide in the deposition area, and is characterized by three distinct source areas, two located on the ~~SW~~south-west side of the landslide and third located on the ~~NE~~north-east side of the landslide. The source and transportation area has an overall length of about 230 m, and a width increasing from 10 to 40 m from the top of the source area to the bottom of the transportation area. Elevation in the landslide ranges from 276 m along the landslide crown, to 206 m at the lowest tip of the deposit. The source and transportation area is bounded locally by sub-vertical, 2 to 4-m high escarpments. In the landslide, terrain slope averages 11°, and is steeper (12°) in the source and transportation area than in the deposition area (9°). The landslide signature (Pike, 1988) is different in the different parts of the landslide. In the source and transport area the signature is predominantly photographical (radiometric), whereas in the landslide deposit it is mainly morphometric (topographic). The differences allow to separate the source and transportation area from the deposition area.

3 Image acquisition

On 14 April 2014, we conducted an aerial survey of the Assignano landslide using a "X" shaped frame octocopter with eight motors mounted on four arms (four sets of CW and CCW props) with a payload capacity of around one kilogram, and a flight autonomy of about 20 minutes. The UAV was equipped with a remotely controlled gimbal hosting a ©GoPro Hero 3 video camera and a Canon EOS M camera. We controlled the flight of the UAV manually, relaying on the real-time video stream provided by the ©GoPro. We kept the operational flight altitude of the UAV in the range between 70 and 100 m above the ground. This allowed the Canon EOS M camera to capture 97 digital colour images of the landslide area with a ground resolution of about 2-4 cm, with the single images having an overlap of about 70% and a side-lap of about 40%. For the accurate geocoding of the images, we positioned 13 red-and-white, four-quadrants square targets, 20 cm × 20 cm in size, outside and inside the landslide. We obtained the geographical location (latitude, longitude, elevation) of the 13 target centres using a Real Time Kinematic (RTK) Differential Global Positioning System (DGPS), with a horizontal error of less than 3 cm. We processed the 97 images using commercial, structure-from-motion software to obtain (i) a 3D point cloud, (ii) a Digital Surface Model (DSM), and (iii) a digital, monoscopic, ultra-resolution (ground sampling distance is 3 × 3 cm) ortho-rectified image in the visible spectral range, which we used for the visual mapping of the Assignano landslide (**Table 1**).

To map the landslide, we also used a stereoscopic pair of ~~very-high resolution (~~VHR~~)~~ images taken on 14 April 2014 i.e., the same day of the UAV survey, by the WorldView-2 satellite that operates at an altitude of 496 km, and collects 46-cm panchromatic, and 1.~~85~~84-m eight-band, multispectral (coastal blue, blue, green, yellow, red, red edge, and near infrared-1, near-infrared-2) imagery at 11-bit dynamic range, in the spectral range 0.400 – 1.040 μm. For the satellite imagery, the rational polynomial coefficients (RPCs) are available, allowing for accurate photogrammetric processing of the images. We used the RPCs to generate 3D models of the terrain from the stereoscopic image pair. Exploiting the characteristics of the satellite image, we prepared four separate images for landslide mapping, namely, (i) a monoscopic, "true colour" (TC) image, (ii) a monoscopic false-colour-composite (FCC) image obtained from the composite near infrared, red and green (~~432~~band 4,3,2), (iii) a TC stereoscopic pair, and (iv) a FCC stereoscopic pair. We prepared separate maps of the Assignano landslide through the visual interpretation of the four images (**Table 1**). Both satellite and UAV images are free from deep shadows (**Fig. 2**).

To compare the images obtained by the UAV and the WorldView-2 satellite, we co-registered the images, and we evaluated the co-registration on seven control points~~,~~ (**Fig. 3**), obtaining a Distance Root Mean Square error, DRMS = 0.53 m, and a Circular Error Probability, $CEP_{50\%}$ = 0.42 m, which we consider adequate for landslide mapping, and for the map comparison.

4 Landslide mapping

We prepared eight maps of the Assignano landslide using different approaches, images and datasets, including two maps prepared through field surveys, four maps prepared through the visual interpretation of monoscopic and stereoscopic satellite images, and two maps prepared through the visual interpretation of the orthorectified images taken ~~during~~by the UAV ~~survey~~ (**Table 1**).

The field mapping and the image interpretation were carried out by independent geomorphologists. The two geomorphologists who carried out the field activities i.e., the reconnaissance field mapping and the RTK-DGPS survey, were not involved in the visual interpretation of the satellite and the UAV images. Equally, the geomorphologist who interpreted visually the satellite and the UAV images did not take part in the field activities. Visual interpretation of the remotely-sensed images was performed by a single geomorphologist to avoid problems related to different interpretation skills by different interpreters (Carrara et al., 1992). We then compared the eight resulting maps of the Assignano landslide adopting a pairwise approach to quantify and evaluate the mapping differences.

The geomorphologist who interpreted visually the images was shown first the 1.84-m resolution, monoscopic satellite image, next the 1.84-m resolution stereoscopic satellite pair, and lastly the 3-cm resolution UAV images. The monoscopic and the stereoscopic satellite images were first shown in TC and then in FCC. Lastly, the interpreter was shown the draped ultra-resolution UAV image. Selection of the sequence of the images given to the geomorphologist for the expert driven visual interpretation was based on the assumption that for landslide mapping (i) the ultra-resolution monoscopic images provide more information than the ~~2~~1.84-m monoscopic or stereoscopic images, (ii) for equal spatial resolution images, stereoscopic images provide more information than monoscopic images, and (iii) for equal image type (monoscopic, stereoscopic), the FCC images provide more information than the TC images. To prevent biases related to a possible previous knowledge of the landslide, the interpreter was not shown the results of the reconnaissance field mapping.

4.1 Field mapping

Field mapping of the Assignano landslide consisted in two synergic activities, (i) a reconnaissance field survey, and (ii) a RTK DGPS aided survey. First, the reconnaissance field survey was conducted by two geomorphologists (FF and MR) who observed the landslide and took photographs of the slope failure from multiple viewpoints, close to and far from the landslide. The geomorphologists draw in the field a preliminary map~~-~~ of the landslide~~ in the field~~ exploiting the most recent satellite image available at the time in Google Earth™, which was taken on 8 July 2013 i.e~~.,~~. **(Fig. 4)**, before the landslide occurred. The reconnaissance ~~filed~~field mapping was then refined in the laboratory using the ground photographs taken in the field. We refer to this reconnaissance representation of the Assignano landslide as "Map B".

Next, the same two geomorphologists (FF and MR) conducted an RTK DGPS aided survey walking a Leica Geosystems GPS 1200 receiver along the landslide boundary, capturing 3D geographic coordinates every about 5 m, in 3D distance. For the purpose, we used the SmartNet ItalPoS real-time network service to transmit the correction signal from the GPS base station to the GPS roving station. The estimated accuracy obtained for each survey point measured along the landslide boundary was 2 to 5 cm, measured by the root mean square error (~~RMS~~RMSE), on the ETRF-2000 reference system. We refer to the cartographic representation of the Assignano landslide produced by the RTK DGPS survey as "Map A". We consider this map as the "ground truth", and we use it as a benchmark against which to compare the other maps. We acknowledge that mapping a landslide by walking a GPS receiver around its boundary is an error prone operation e.g., because in places the landslide boundary is not sharp, or clearly visible from the ground (Santangelo et al., 2010). However, we maintain this is the most reasonable working assumption, and that the geometrical information obtained by walking a GPS receiver along the landslide boundary was superior to the information obtained through the reconnaissance field mapping (Map B) (Santangelo et al., 2010).

4.2 Mapping through image interpretation

A trained geomorphologist (MS) used the three monoscopic images (i.e., the TC and FCC monoscopic satellite images, and the monoscopic ultra-resolution UAV image) to perform a heuristic, visual mapping of the Assignano landslide. For ~~the~~this purpose, the interpreter considered the photographic (colour, tone, mottling, texture) and geometrical (shape, size, curvature, pattern of individual terrain features, or sets of features) characteristics of the images (Antonini et al., 1999). In this way, the geomorphologist prepared (i) "Map C" interpreting visually the monoscopic, TC satellite image, (ii) "Map D" interpreting visually the monoscopic, FFC satellite image, and (iii) "Map G" interpreting visually the monoscopic, TC UAV image (**Table 1**).

Next, the interpreter used the two stereoscopic satellite images (i.e., the TC and FCC images) to prepare "Map E" and "Map F" (**Table 1**). In the stereoscopic images, the photographic and morphological information is combined, favouring the recognition of the landslide features through the joint analysis of photographic (colour, tone, mottling, texture), geometrical (shape, size, pattern of features), and morphological terrain features (curvature, convexity, concavity). To analyse visually the stereoscopic satellite images, the interpreter used the StereoMirror™ hardware technology, combined with the ERDAS IMAGINE® and Leica Photogrammetry Suite (LPS) software. To map the landslide features in real-world, 3D geographical coordinates, the interpreter used a 3D floating cursor (Fiorucci et al., 2015).

To interpret the ultra-resolution UAV image, the interpreter overlaid ("draped") the image on Google Earth™. For the purpose, we first treated the UAV image with gdal2tiles.py software to obtain a set of image tiles compatible with the Google Earth™ terrain visualization platform~~, and we used the platform standard editing tools to digitize the landslide features.~~. To interpret visually the ultra-resolution UAV image, the interpreter overlaid ("draped") the image on Google Earth™. For the purpose, we first treated the UAV image with the gdal2tiles.py software to obtain a set of image tiles compatible with Google Earth™ terrain visualization platform. To the best of our knowledge, the platform is the only free, 2.5D image visualisation environment that allows the editing of vector (i.e., point, line, polygon) information. Other commercial (e.g., ArcScene) and open source (e.g., ParaView, GRASS GIS), 2.5D visualization tools do not provide editing capabilities. Google Earth™ is a user-friendly solution for mapping single landslides, and for preparing landslide event inventories for limited areas, with the possibility for the user to visualize a landscape from virtually any viewpoint, facilitating landslide mapping. We refer to the representation of the Assignano landslide obtained through the visual interpretation of the ultra-resolution UAV image as “Map H”.

For the visual interpretation of the satellite and the UAV images, the interpreter adopted a visualization scale in the range from 1:1000 to 1:6000, depending on the image spatial resolution (**Table 1**). The scale of observation was selected to obtain the best readability of each landslide feature and the surroundings, which is a common practice in image visual analysis for landslide mapping (Fiorucci et al., 2011). Hence, even if the maps were produced at slightly different observation scales, the differences arising from the comparison are due to actual features (i.e., the image resolution and radiometry), and not to the different observation scales.

5 Results

Using the described mapping methods, and the available satellite and UAV images (**Table 1**), we prepared eight separate and independent cartographic representations of the Assignano landslide, shown in **Fig.** ~~2~~5 as Map A to Map H.

Considering the entire landslide, visual inspection of **Fig.** ~~2~~5 reveals that the maps most similar to the benchmark (Map A) are Map E, prepared examining the true colour (TC) stereoscopic satellite image, and Map F, prepared examining the false colour composite (FCC) stereoscopic satellite image. Conversely, the largest differences were observed for the landslide maps obtained through the reconnaissance field survey (Map B), and the visual interpretation of the monoscopic satellite images (Map C and Map D). Considering only the source and transportation areas (dark colours in **Fig.** ~~2~~5), interpretation of the UAV ultra-resolution images resulted in the landslide maps most similar (Map G and Map H) to the benchmark (Map A). It is worth noticing the systematic lack in the mapping of one of the two secondary landslide source areas located in the SW side of the landslide, which was recognized only from the visual inspection of the ultra-resolution orthorectified images taken by the UAV ~~flight~~. In the field, this source area was characterized by small cracks along the escarpment and a limited disruption of the meadow, making it particularly difficult to detect and map. We argue that only the ultra-resolution images allowed for the detection of the cracks. Considering only the landslide deposit (light colours in **Fig.** ~~2~~5), the landslide mapping that was more similar to the benchmark (Map A) was obtained interpreting the TC, stereoscopic satellite images (Map E). We also note that in most of the maps the landslide deposit was mapped larger (Map G, Map H) or much larger (Map B, Map C and Map D) than the benchmark (Map A).

Table 2 lists geometric measures of the mapped landslides, including the planimetric measurement of length, width, and area (i) of the entire landslide, (ii) of the landslide source and transportation area (dark colours in **Fig.** 25), and (iii) of the landslide deposit (light colours in **Fig.** 25). The length and width measurements were obtained in a GIS as the length and the width of the minimum oriented rectangle encompassing (i) the entire landslide, (ii) the landslide source and transportation area, and (iii) the landslide deposit. Our benchmark (Map A) has a total area $A_L = 1.1 \times 10^4$ m^2, and is $L_{LS} = 362$ m long and $W_{LS} = 71$ m wide. Amongst the other seven maps (Map B to Map H in **Fig.** 25), the largest landslide is shown in Map B, obtained through the reconnaissance field mapping, and has $A_L = 1.91 \times 10^4$ m^2, 71.1% larger than the benchmark. Conversely, the smallest landslide is shown in Map F, with $A_L = 1.1 \times 10^4$ m^2, 4.6% smaller than the benchmark. The longest and largest landslide is found in Map C, with $L_{LS} = 405$ m (11% longer than the benchmark) and $W_{LS} = 113$ m (60% wider than the benchmark).

Considering the source and transportation area, in Map A (the benchmark) $A_{LS} = 5.4 \times 10^3$ m^2, $L_{LS} = 228$ m, and $W_{LS} = 52$ m. The largest representation of the source and transportation area is found in Map B (reconnaissance field mapping) with $A_{LS} = 7.4 \times 10^3$ m^2, 36.9% larger than the benchmark, and the smallest source and transportation area is found in Map G, with $A_{LS} = 5.2 \times 10^3$ m^2, 3.6% smaller than the benchmark. The longest source and transportation area is found in Map F, with $L_{LS} = 239$ m, 5% longer than the benchmark, and the shortest source and transportation area is shown in Map C, with $L_{LS} = 206$ m, 9.7% shorter than the benchmark. The largest source and transportation area is shown in Map B, $W_{LS} = 60$ m, 15.7% wider than Map A, and the narrowest source and transportation area is in Map C, $L_{LS} = 44$ m, 15.3% narrower than the benchmark. Considering instead only the landslide deposit, our benchmark (Map A) has $A_{LD} = 5.7 \times 10^3$ m^2, $L_{LS} = 153$ m, and $W_{LS} = 61$ m. The largest deposit is shown in Map B (reconnaissance field mapping) and has $A_{LD} = 1.2 \times 10^4$ m^2, 103.4% larger than the benchmark, whereas the smallest landslide deposit is shown in Map F, with $A_{LD} = 4.6 \times 10^3$ m^2, 19.8% smaller than the benchmark. Analysis of the length and width of the landslide deposit reveals that Map C shows the longest deposit, $L_{LS} = 206$ m, 35% longer than the benchmark, and Map H shows the shortest deposit, $L_{LS} = 122$ m, 20.2% shorter than the benchmark. Similarly, the largest landslide deposit is shown in Map C, $W_{LS} = 112$ m, 82.8% wider than the benchmark, and the narrowest landslide deposit is portrayed in Map E, W_{LS} = 56 m, 8.2% less than the benchmark.

To compare quantitatively the different landslide maps, we use the error index *E* proposed by Carrara et al. (1992), adopting the pairwise comparison approach proposed by Santangelo et al. (20152015a). The index provides an estimate of the discrepancy (or similarity) between corresponding polygons in two maps, and is defined as:

$$E = \frac{(A \cup B) - (A \cap B)}{(A \cup B)};\ 0 \le E \le 1, \tag{1}$$

where, A and B are the areas of two corresponding polygons in the compared maps, and ∪ and ∩ are the geographical (geometric) union and intersection of the two polygons, respectively. *E* spans the range from 0 (perfect matching) to 1 (complete mismatch).

We compared the eight maps of the Assignano landslide (**Fig. 25**) adopting a pairwise approach, and considering first only the landslide source and transportation area, next only the landslide deposit, and lastly the entire landslide. **Fig. 36** summarizes the 84 values of the error index *E*, 28 for the landslide source and transportation area (**Fig. 36 I**), 28 for the landslide deposit (**Fig. 36 II**), and 28 for the entire landslide (**Fig. 36 III**). On average, the source and transportation area exhibits values of the error index smaller than the values found in the landslide deposit. This indicates that in the source and transportation area the landslide maps are more similar than in the landslide deposit. Inspection of **Fig. 36 I**, reveals a decrease of the error index in the source and transportation area for the maps obtained interpreting the available images (from Map C to Map H), compared to our benchmark obtained through the RTK DGPS survey (0.38 < 15 ≤*E* < ≤0.1538), with Map G obtained interpreting the TC, monoscopic, ultra-resolution UAV image. In the landslide deposit (**Fig. 36 II**), the minimum difference (*E* = 0.21) was found comparing the benchmark to Map E, obtained through the interpretation of the stereoscopic TC satellite image, and the largest difference (*E* = 0.52) was found comparing the benchmark to Map C, prepared interpreting the TC, monoscopic, satellite image.

Comparison of the maps obtained through the interpretation of the monoscopic images (Map C and Map D), and the maps obtained through the interpretation of stereoscopic (Map E and Map F) or ultra-resolution images (Map G and Map H), reveals a generally poor agreementhigh values of the error index, which is slightly worse in the landslide deposit. In particular, 0.31 ≤ *E* ≤ 0.44This is evident in the source and transportation area (0.31 ≤ *E* ≤ 0.44) (**Fig. 3I 6 I**), and 0.43 ≤ *E* ≤ 0.63 in the landslide deposit ($0.43 \leq E \leq 0.63$) (**Fig. ~~3H~~6 II**). Map C and Map D are very similar, with a mapping error $E = 0.17$. Maps obtained through the interpretation of stereoscopic satellite images (Map E and Map F, prepared using TC and FCC images, respectively), and maps prepared by interpreting the UAV images (Map G and Map H), exhibit a generally ~~good agreement.~~low value of E. In particular, $0.14 \leq E \leq 0.26$ in the landslide source and transportation area, and $0.15 \leq E \leq 0.38$ in the landslide deposit. The reconnaissance field mapping (Map B) exhibited the largest differences compared to all the other maps ($0.63 \leq E \leq 0.45$) in the landslide source and transportation area, and $0.44 \leq E \leq 0.73$ in the landslide deposit. The large values of E in the landslide deposit is probably due to lack of visibility of part of the landslide toe in the field.

6 Discussion

We discuss the ability of the different images used to detect and map the Assignano landslide (**Fig. 1**) to resolve the landslide photographical and morphological signatures, considering separately the image spatial and spectral resolutions, and the image type i.e., monoscopic, stereoscopic, or pseudo-stereoscopic. We treat each of the three factors separately, keeping the other two factors constant. To evaluate the influence of the image spatial resolution on landslide mapping, we compare to our benchmark (Map A) two true-colour (TC) monoscopic maps (Map C and Map G), and two TC stereoscopic maps (Map E and Map H). Next, to evaluate the influence of the image spectral resolution on the landslide mapping, we compare to the benchmark (Map A) the TC and the false-colour-composite (FCC) monoscopic maps (Map C and Map D), and the corresponding TC and FCC stereoscopic maps (Map E and Map F). Lastly, to assess the influence of the type of image (i.e., monoscopic, stereoscopic, pseudo-stereoscopic) on the landslide mapping, we compare to the benchmark (Map A) the monoscopic (Map C) and the stereoscopic (Map E) TC maps (**Fig. ~~4A~~7A**), the two FCC maps (Map D and Map F) (**Fig. ~~4B~~7B**), and the maps obtained interpreting the ultra-resolution images captured by the UAV (Map G and Map H). **Fig. ~~3~~6** summarizes the mapping errors E obtained by the pairwise comparisons of the eight landslide maps shown in **Fig. ~~2~~5**.

We first evaluate the role of the image spatial resolution in the production of the different maps of the Assignano landslide. Inspection of **Fig. ~~3~~6 I** reveals that the maps of the landslide source and transportation area obtained from images characterized by the highest spatial resolution (i.e., Map G and Map H) exhibits the smallest errors ($E \leq 0.16$), when compared to the benchmark

(Map A). The mapping error obtained for Map C (TC, monoscopic, $E = 0.38$) is 2.5 times larger than the error obtained using the ultra-resolution orhtorectified images taken by the UAV (Map G, $E = 0.15$, and Map H, $E = 0.16$), whereas the error obtained from Map E (TC, stereoscopic, $E = 0.23$) is smaller, and about 1.5 times larger than the error obtained for Map H (TC, pseudo-stereoscopic, $E = 0.16$). In the landslide deposit (**Fig. ~~3~~6 II**), the map obtained exploiting the monoscopic, TC satellite image (Map C) exhibits an error $E = 0.52$, 1.7 times larger than the error obtained using Map G (TC, monoscopic UAV, $E = 0.30$). Conversely, the error is smaller in the map obtained from the 2-m spatial resolution, stereoscopic TC satellite image (Map E, $E = 0.21$) than from the 3-cm spatial resolution, pseudo-stereoscopic image taken by the UAV (Map H, $E = 0.30$). Collectively, the pairwise comparisons highlights ~~a significant~~an improvement of the quality of the mapping of the landslide features that exhibits a distinct photographical signature, most visible in the source and transportation area of the Assignano landslide, with an increase of the image spatial resolution (**Fig. ~~3~~6**). Use of the ultra-resolution image captured by the UAV did not result in ~~a significant~~an improvement of the mapping in the deposition area of the Assignano landslide, where the landslide exhibits a distinct morphological signature. We further observe that most of the landslide parts that were not identified in the maps prepared using the satellite image are covered by vegetation, locally bounded by small and thin cracks with an average width smaller than the size of the 2×2 m pixel. In the satellite image, the cracks are located in pixels containing a mix of vegetation and bare soil, making it difficult for the interpreter to recognize the cracks.

Next, we evaluate the effectiveness of the image spectral resolution, and for the purpose we examine the mapping errors of Maps C and Map E (TC), and of Map D and Map F (FCC). The mapping of the source and transportation area prepared using the false-colour-composite (FCC) images (Map D and Map F) resulted in smaller errors than the mapping prepared using the corresponding true-colour (TC) images (Map C and Map E), for both monoscopic and stereoscopic images (**Fig. ~~3~~6 I**). In the source and transportation area, the false-colour-composite emphasized the presence or absence of the vegetation, and contributed locally to highlight the typical photographical signature of the landslide, which helped the photo-interpreter to detect and map the slope failure. Conversely, in the landslide deposition area (**Fig. ~~3~~6 II**) use of the FCC images did not result in a systematic reduction of the mapping error, when compared to the TC images. We conclude that use of the additional information contributed by the Near Infrared (NIR) band in the 1.84-m resolution satellite image did not improve the quality of the mapping. On the other hand, the contribution of the NIR in the 3-cm UAV image remains unknown.

Next, we evaluate the influence of the image type (i.e., monoscopic, stereoscopic, pseudo-stereoscopic) on the mapping error by comparing (i) the TC images (Map C and Map E), (ii) the FCC images (Map D and Map F), and (iii) the ultra-resolution UAV image (Map G and Map H). Comparison of the TC, monoscopic (Map C) and stereoscopic (Map E) images revealed a mapping error for the entire landslide E = 0.48, with the mismatch ~~significantly~~ larger in the deposition area (E = 0.59) than in the source and transpiration area (E = 0.45) (**Fig. ~~3~~6**). A similar result was obtained comparing the FCC, monoscopic (Map D) and stereoscopic (Map F) images, with a mapping error for the entire landslide E = 0.44, and again the mismatch ~~significantly~~is larger in the deposition area (E = 0.60) than in the source and transpiration area (E = 0.36). In the deposition area, where the morphological signature of the Assignano landslide is strongest, the mapping error obtained comparing our benchmark (Map A) to the landslide maps prepared using the monoscopic images (Map C and Map D) is 2 times larger than the error observed for the maps prepared using the corresponding stereoscopic images (Map E and Map F). The differences are smaller in the source and transportation area, where the morphological signature of the landslide is less distinct. Direct comparison of Map E (TC, stereoscopic) and Map F (FCC, stereoscopic) for the entire landslide reveals a very small mapping error (E = 0.15), indicating the similarity of the two maps, which were also very similar to the benchmark (Map A), $E \leq 0.20$.

Comparison for the entire landslide of the maps prepared using the ultra-resolution images captured by the UAV (Map G and Map H) exhibits the smallest error of all the pairwise comparisons (E = 0.08) (**Fig. ~~3~~6 III**), indicating the large degree of matching between the two maps. The degree of matching is only marginally smaller in the source and transportation area, and in the deposition area (E = 0.15). When compared to our benchmark (Map A), Map G and Map H exhibit a small error (E = 0.19) for the entire landslide, which is larger in the deposition area ($E \leq 0.30$) and slightly smaller in the source and transport area ($E \leq 0.15$). Interestingly, the mismatch with Map A (the benchmark) is lower for the monoscopic (Map G) than for the pseudo-stereoscopic (Map H) map. The finding highlights the lack of an advantage in using a pseudo-stereoscopic (2.5D) image for mapping the Assignano landslide. We attribute this result to the low resolution of the (pre-event) DEM used to drape the ultra-resolution image for visualization purposes, which did not add any significant morphological information to the expert visual interpretation.

Joint analysis of **Fig. ~~2B~~5B** and **Fig. ~~3~~6** reveals that, when compared to our benchmark (Map A), the reconnaissance field mapping (Map B) exhibited the largest mapping error of all the performed pairwise comparisons, with *E* = 0.45 in the source and transportation area, *E* = 0.67 in the landslide deposit, and *E* = 0.55 for the entire landslide. We note than an error of *E* = 0.50 indicates that 50% of the landslide area in one map (Map B, in this case) does not overlay with the other map (Map A, the benchmark, in this case). Our results are similar to the results of tests performed to compare field-based landslide maps against GPS-based surveys of single landslides (Santangelo et al., 2010), the visual interpretation of very-high resolution stereoscopic satellite images (Ardizzone et al., 2013), or the semi-automatic processing of monoscopic satellite images (Mondini et al., 2013), and confirm the inherent difficulty in preparing accurate landslide maps in the field, unless the mapping is supported by a GPS survey or a similar technology.

Our experiment showed that the mapping of the Assignano landslide obtained exploiting the ultra-resolution images captured by the UAV (Map G and Map H) was comparable to the maps obtained using the high resolution stereoscopic satellite image (Map E and Map F), and to the ground-based RTK DGPS survey (Map A, the benchmark). We conclude that ultra-resolution images captured by an UAV and the stereoscopic satellite images are well suited to map event landslides, at least in physiographical settings similar to the one of our study area, and for landslides similar to the Assignano landslide (**Fig. 1**).

For event landslide mapping, selection between ultra-resolution pseudo-stereoscopic UAV images and very-high resolution stereoscopic satellite images depends on (i) the extent of the investigated area, (ii) the available resources, including time and budget, and (iii) the accessibility to the study area. The selection is largely independent from the landslide signature, at least for landslides similar to the Assignano landslide. From an operational perspective, modern multi-rotor UAVs allow for the acquisition of ultra-resolution images over small areas in a limited time, and at very low costs. UAV-based surveys are flexible in their acquisition planning, and partly independent from the local lighting conditions, including the cloud cover. As a drawback, UAVs are strongly (and negatively) affected by wind speed and weather conditions, they allow for a limited flight time (currently approximately 20 minutes in optimal conditions), which is reduced in bad weather conditions and in cold environments, and ~~a have~~ typically have limited data storage capacity. Further, it must be possible for the pilot to be at the same time near to the area to be surveyed and to maintain a safe distance from the UAV, a condition that may be difficult to attain in remote or in mountain areas. Collectively, the intrinsic advantages and limitations of modern UAVs make the technology potentially well suited for the acquisition of ultra-resolution images for event, seasonal, and multi-temporal mapping of single landslides, of multiple landslides in a single slope, or in a relatively small area (a few hectares). The use of UAV images was recently proposed by Turner et al. (2015) for determining the landslide dynamics, exploiting time series of images that can be constructed using UAVs. The result is achievable thanks to centimetre co-registration accuracy of the UAV images. Use of UAVs becomes impracticable with the increasing extent of the study area, largely due to (i) the operational difficulty of ~~flaying~~flying UAVs over large areas~~,~~ (more than a few square kilometres), and (ii) the acquisition and image processing time and associated cost, which increase rapidly with the size of the study area (**Table 3**). On the other hand, very-high resolution, stereoscopic satellite images have also advantages and limitations for the production of event, seasonal and multi-temporal landslide inventory maps (Guzzetti et al., 2012). The main advantage of the satellite images is that they cover large or very areas (tens to hundreds of square kilometres) in a single frame with a sub-~~metric~~metre resolution well suited for landslide mapping through the expert visual interpretation of the images (Ardizzone et al., 2013). On the other hand, limitations remain due to distortions caused by different off-nadir angles in successive scenes, and to difficulties – in places severe – to obtaining suitable (e.g., cloud-free) images at the required time intervals. This is particularly problematic for the production of seasonal and multi-temporal landslide maps.

Information on the photographic or ~~topographic~~morphological signature of the typical, or most abundant, landslides in an area, is important to ~~help select~~selecting the optimal characteristics of the images best suited for the production of an event, seasonal or multi-temporal landslide inventory map. Use of images of non-optimal characteristics for a typical landslide signature in an area may condition the quality (i.e., completeness, ~~geographic~~positional and thematic accuracy) of the landslide inventory. Where possible, we recommend that the acquisition of ~~the~~ images used for the production of event, seasonal or multi-temporal landslide inventory maps is planned considering the typical landslide signature, in addition to the ~~scope~~purpose (event inventory, planning of monitoring systems), scale of the mapping~~,~~ (i.e. regional or slope scale), and the size and complexity of the study area (**Table 3**).

7 Concluding remarks

We executed an experiment aimed at determining and measuring the effects of the image characteristics on event landslide mapping. In the experiment, we compared landslide maps obtained (i) through the expert visual interpretation of an ultra-resolution image taken by an UAV with a ground resolution of 3 × 3 cm, and monoscopic and stereoscopic true-colour and false-colour-composite (1.84 × 1.84 m) images taken by the WorldView-2 satellite, (ii) a reconnaissance field survey of the landslide, and (iii) an accurate survey of the landslide obtained by walking a GPS receiver along the landslide boundary. We conducted the experiment on a the Assignano landslide (**Fig. 1**) triggered by intense rainfall in December 2013 in the northwest-facing slope of the Assignano village, Umbria, central Italy. The landslide exhibited a predominant photographical (radiometric) signature in the source and transport area, and a more distinct morphological (topographic) signature in the deposition area. The results of our mapping experiment allow for the following conclusions.

First, in the landslide source and transport area, where the signature of the slope failure was primarily photographical (radiometric), mapping errors (Carrara et al., 1992; Santangelo et al., ~~2015~~2015a) decreased with the increase of the spatial resolution of the images used for the expert visual detection and mapping of the landslide. In the same area, the image photographic (radiometric) characteristics (true-colour, false-colour-composite) and the image type (monoscopic, stereoscopic) played a minor role in augmenting the quality of the landslide map. Conversely, in the deposition area, where the signature of the landslide was primarily morphological (topographical), mapping errors decreased using stereoscopic satellite images that allowed detecting topographic features distinctive of the landslide. ~~In the same area, a better spatial and spectral resolution did not contribute significantly to reducing the mapping errors.~~

FCC and TC in the stereoscopic satellite images give similar values of the error. This indicates that the spectral resolution of the images does not provide useful information to recognize and map the landslide morphological features. On the other hand, the high spatial resolution provided by the UAV images reduces the error, when compared to the monoscopic satellite imagery. However, the error obtained using the UAV images remains higher than that obtained using stereoscopic satellite images, despite the latter having a pixel one order of magnitude larger than the UAV images. We conclude that the increase in the spatial resolution improves the ability to map morphological features when using monoscopic images.

Second, use of the stereoscopic satellite images resulted in more accurate landslide maps (lower error index *E*) than the corresponding monoscopic images in the landslide deposition area, where the signature of the landslide was primarily morphometric (topographic). This was expected, as the stereoscopic vision allowed to better capture the 3D terrain features typical of a landslide (Pike, 1988), including curvature, convexity and concavity. Conversely, visual examination of the false-colour-composite images resulted in more accurate maps than the corresponding true-colour images in the landslide source and transport area, where the signature of the landslide was primarily photographic (radiometric). This was also expected (Guzzetti et al., 2012). Expert visual interpretation of pseudo-stereoscopic ultra-resolution image failed to provide better results than the corresponding monoscopic ultra-resolution image, most probably because the DEM used to drape (overlay) the image on the terrain information was of low resolution.

Third, the ultra-resolution (3 × 3 cm) image captured by the photographic camera flown on-board the Unmanned Aerial Vehicle (UAV) proved to be very effective to detect and map the landslide. The expert visual interpretation of the monoscopic ultra-resolution image provided mapping results comparable to those obtained using the about 2-m resolution, stereoscopic satellite image.

Fourth, a comparative analysis of the technological constrains and the costs of acquisition and processing of ultra-resolution imagery taken by UAV, and of high, or very-high resolution imagery taken by optical satellites, revealed that the ultra-resolution images are well suited to map single event landslides, clusters of landslides in a single slope, or a few landslides in nearby slopes in a small area (up to few square kilometres, Giordan et al., 2017) , and prove unsuited to cover large~~,~~ and very large areas where the stereoscopic satellite images provide the most effective option~~.~~ (Boccardo et al., 2015).

Fifth, our field-based reconnaissance mapping (Map B) provided the least accurate mapping results, measured by the largest mapping error (*E* = 0.55 for the entire landslide) when compared to the benchmark map (**Fig. ~~3~~6**). Our results confirm the inherent difficulty in preparing accurate landslide maps in the field through a reconnaissance mapping (Santangelo et al., 2010).

Although we conducted our study on a single landslide (**Fig. 1**), we maintain that the findings are general, and can be useful to decide on the optimal imagery and technique to be used when planning the production of a landslide inventory map. We emphasize that the technique and imagery used to prepare landslide inventory maps should be selected depending on multiple factors, including (i) the typical or predominant landslide signature (photographic or morphological), (ii) the scale and size of the study area (a single slope, a small catchment, a large region), and (iii) the scope of the mapping (event, seasonal, multi-temporal, Guzzetti et al., 2012).

8 Acknowoledgements

FF and MS were supported by a grant of Italian Dipartimento della Protezione Civile. We thank Andrea Bernini and Mario Truffa, Servizio Protezione Civile della Città Metropolitana di Torino, for flying the UAV over the Assignano landslide.

9 References

Allasia, P., Manconi, A., Giordan, D., Baldo, M., and Lollino, G.: ADVICE: a new approach for near-real-time monitoring of surface displacements in landslide hazard scenarios. Sensors, 13, 7, 8285-8302, https://doi.org/10.3390/s130708285, 2013.

~~Allum, J. A. E.: Photogeology and regional mapping. Pergamon, 107 pp., 1966.~~

Antonini, G., Ardizzone, F., Cardinali, M., Galli, M., Guzzetti, F. and Reichenbach, P.: Surface deposits and landslide inventory map of the area affected by the 1997 Umbria-Marche earthquakes, Boll. Soc. Geol. It., 121, 843-853, 2002.

Ardizzone, F., Cardinali, M., Carrara, A., Guzzetti, F., and Reichenbach, P.: Impact of mapping errors on the reliability of landslide hazard maps, Nat. Hazards Earth Syst. Sci., 2, 3-14, https://doi.org/10.5194/nhess-2-3-2002, 2002.

Ardizzone, F., Cardinali, M., Galli, M., Guzzetti, F., and Reichenbach, P.: Identification and mapping of recent rainfall-induced landslides using elevation data collected by airborne Lidar, Nat. Hazards Earth Syst. Sci., 7, 637-650, https://doi.org/10.5194/nhess-7-637-2007, 2007.

Ardizzone, F., Fiorucci, F., Santangelo, M., Cardinali, M., Mondini, A.C., Rossi, M., Reichenbach, P., and Guzzetti, F.: Very-high resolution stereoscopic satellite images for landslide mapping. C. Margottini, P. Canuti, K. Sassa (Eds.), Landslide Science and Practice, Landslide Inventory and Susceptibility and Hazard Zoning, 1, Springer, Heidelberg, Berlin, New York, 95–101, https://doi.org/10.1007/978-3-642-31325-7_12, 2013.

Boccardo, P., Chiabrando, F., Dutto, F., Tonolo, F.G., Lingua, A.: UAV deployment exercise for mapping purposes: evaluation of emergency response applications. Sensors, 15, 15717-15737, 2015, https://doi.org/10.3390/s150715717.

Brardinoni, F., Slaymaker, O., and Hassan, M.A.: Landslides inventory in a rugged forested watershed: a comparison between air-photo and field survey data, Geomorphology, 54, 179-196, https://doi.org/10.1016/S0169-555X(02)00355-0, 2003.

Carrara, A., Cardinali, M., and Guzzetti, F.: Uncertainty in assessing landslide hazard and risk, ITC Journal, 2, 172-183, 1992.

Di Maio, C., and Vassallo, R.: Geotechnical characterization of a landslide in a Blue Clay slope, Landslides, 8, 17-32, https://doi.org/10.1007/s10346-010-0218-8, 2011.

Fiorucci, F., Cardinali, M., Carlà, R., Rossi, M., Mondini, A. C., Santurri, L., Ardizzone, F., and Guzzetti, F.: Seasonal landslides mapping and estimation of landslide mobilization rates using aerial and satellite images, Geomorphology, 129, 59-70, https://doi.org/10.1016/j.geomorph.2011.01.013, 2011.

Fiorucci, F.; Ardizzone, F.; Rossi, M.; Torri, D.: The Use of Stereoscopic Satellite Images to Map Rills and Ephemeral Gullies. Remote Sens., 7, 14151-14178, https://doi.org/10.3390/rs71014151, 2015.

Galli, M., Ardizzone, F., Cardinali, M., Guzzetti, F., and Reichenbach, P.: Comparing landslide inventory maps, Geomorphology, 94, 268–289, https://doi.org/10.1016/j.geomorph.2006.09.023, 2008.

Giordan, D., Allasia, P., Manconi, A., Baldo, M., Santangelo, M., Cardinali, M., Corazza, A., Albanese, V., Lollino, G., and Guzzetti, F.: Morphological and kinematic evolution of a large earthflow: The Montaguto landslide, southern Italy, Geomorphology, 187, 61-79, https://doi.org/10.1016/j.geomorph.2012.12.035, 2013.

Giordan, D., Manconi, A., Allasia, P., and Bertolo, D.: Brief Communication: On the rapid and efficient monitoring results dissemination in landslide emergency scenarios: the Mont de La Saxe case study, Nat. Hazards Earth Syst. Sci., 15, 2009-2017, https://doi.org/10.5194/nhess-15-2009-2015, ~~2015~~2015a.

Giordan, D., Manconi, A., Facello, A., Baldo, M., dell'Anese, F., Allasia, P., and Dutto, F.: Brief Communication: The use of an unmanned aerial vehicle in a rockfall emergency scenario, Nat. Hazards Earth Syst. Sci., 15, 163-169, https://doi.org/10.5194/nhess-15-163-2015, ~~2015~~2015b.

Giordan, D., Manconi, A., Remondino, F., Nex, F.: Use of unmanned aerial vehicles in monitoring application and management of natural hazards, Geomatics, natural hazards and risk, 8(1), 1-4, 2017.

Gokceoglu, C., Sonmez, H., Nefeslioglu, H. A., Duman, T. Y., Can, T.: The 17 March 2005 Kuzulu landslide (Sivas, Turkey) and landslide-susceptibility Map of its near vicinity. Engineering Geology, 81, 1, 65-83, https://doi.org/10.1016/j.enggeo.2005.07.011, 2005.

Guzzetti, F., ~~Ardizzone, F., Cardinali, M., Rossi, M., and Valigi, D.: Landslide volumes and landslide mobilization rates in Umbria, central Italy, Earth Planet. Sc. Lett., 279, 222-229, https://doi.org/10.1016/j.epsl.2009.01.005, 2009.~~

~~Guzzetti, F.,~~ Cardinali, M., Reichenbach, P., Cipolla, F., Sebastini, C., Galli, M., and Salvati, P.: Landslides triggered by the 23 November 2000 rainfall event in the Imperia Province, Western Liguria, Italy, Eng. Geol., 73, 229–245, https://doi.org/10.1016/j.enggeo.2004.01.006, 2000.

Guzzetti, F., Mondini, A. C., Cardinali, M., Fiorucci, F., Santangelo, M., and Chang, K.-T.: Landslide inventory maps: new tools for and old problem, Earth-Sci. Rev., 112, 42-66, https://doi.org/10.1016/j.earscirev.2012.02.001, 2012.

Haneberg, W. C., Cole, W. F., and Kasali, G.: High-resolution lidarbased landslide hazard mapping and modeling, UCSF Parnassus Campus; San Francisco, USA, B. Eng. Geol. Environ., 68, 263-276, https://doi.org/10.1007/s10064-009-0204-3, 2009.

~~Keaton, J. R. and DeGraff, J. V.: Surface observation and geologic mapping, in: Landslides: Investigation and Mitigation, Transportation Research Board, Washington, D.C., 178-230, 1996.~~

Hutchinson, J. N.: A coastal mudflow on the London clay cliffs at Beltinge, North Kent, Geotechnique, 24, 412–438, 1970.

Manconi, A., Casu, F., Ardizzone, F., Bonano, M., Cardinali, M., De Luca, C., Gueguen, E., Marchesini, Parise, M., Vennari C., Lanari, R., Lanari, R.: Brief Communication: Rapid mapping of landslide events: the 3 December 2013 Montescaglioso landslide, Italy. Natural Hazards and Earth System Sciences, 14, 7, 1835, https://doi.org/10.5194/nhess-14-1835-2014, 2014.

~~Miller, C. V., Photogeology. Mac Graw Hill Book Company Inc., London, 1961.~~

Mondini, A. C., Marchesini, I., Rossi, M., Chang, K.-T., Pasquariello, G., and Guzzetti, F.: Bayesian framework for mapping and classifying shallow landslides exploiting remote sensing and topographic data, Geomorphology, 201, 135-147, https://doi.org/10.1016/j.geomorph.2013.06.015, 2013.

Monserrat, O. and Crosetto, M.: Deformation measurement using terrestrial laser scanning data and least squares 3D surface matching. ISPRS J. Photogramm., 63(1), 142–154, https://doi.org/10.1016/j.isprsjprs.2007.07.008, 2008.

Niculiţă, M.: Automatic landslide length and width estimation based on the geometric processing of the bounding box and the geomorphometric analysis of DEMs, Nat. Hazards Earth Syst. Sci., 16, 2021-2030, https://doi.org/10.5194/nhess-16-2021-2016, 2016.

~~Notti, D., Davalillo~~Niethammer, U., S. Rothmund, M. R. James, Travelletti, J. ~~C., Herrera, G.,~~ and ~~Mora, O.: Assessment~~Joswig M.: UAV based remote sensing of landslides, Int. Arch. Photogram. Remote Sensing Spatial Info. Sci., ~~the performance~~38(5), 496-501, 2010.

Petschko, H.; Bell, R. Glade, T.: Effectiveness of ~~X-band satellite radar data~~visually analyzing LiDAR DTM derivatives for ~~landslide~~earth and debris slide inventory mapping ~~and monitoring: Upper Tena Valley case study, Nat. Hazards Earth Syst~~for statistical susceptibility modeling, Landslides 13(5), 857-872, 2016~~. Sci., 10, 1865-1875~~, https://doi.org/10.~~5194/nhess-10-1865-2010, 2010~~1007/s10346-015-0622-1.

Pike, R.J.: The geometric signature: quantifying landslide-terrain types from digital elevation models, Mathematical Geology, 20, 5, 491-511, 1988.

Plank, S.: Rapid damage assessment by means of multi-temporal SAR—A comprehensive review and outlook to Sentinel-1, Remote Sensing, 6, 6, 4870-4906, https://doi.org/10.3390/rs6064870, 2014.

~~Ray, R. G.: Aerial Photographs in Geological Interpretation and Mapping. Geological Survey Professional Paper 373, Washington, USA, 1960.~~

Razak, K. A., Santangelo, M., Van Westen, C. J., Straatsma, M. W., and de Jong, S. M.: Generating an optimal DTM from airborne laser scanning data for landslide mapping in a tropical forest environment, Geomorphology, 190, 112-125, https://doi.org/10.1016/j.geomorph.2013.02.021, 2013.

Rosi, A., Vannocci, P., Tofani, V., Gigli, G., Casagli, N.: Landslide characterization using satellite interferometry (PSI), geotechnical investigations and numerical modelling: the case study of Ricasoli Village (Italy). Int. J. Geosci., 4, 904-918, https://doi.org/10.4236/ijg.2013.45085, 2013.

Santangelo, M., Cardinali, M., Rossi, M., Mondini, A. C., and Guzzetti, F.: Remote landslide mapping using a laser rangefinder binocular and GPS, Nat. Hazards Earth Syst. Sci., 10, 2539-2546, https://doi.org/10.5194/nhess-10-2539-2010, 2010.

Santangelo, M., Marchesini, I., Bucci, F., Cardinali, M., Fiorucci, F., and Guzzetti, F.: An approach to reduce mapping errors in the production of landslide inventory maps, Nat. Hazards Earth Syst. Sci., 15, 2111-2126, https://doi.org/10.5194/nhess-15-2111-2015, ~~2015~~2015a.

Santangelo, M., Marchesini, I., Cardinali, M., Fiorucci, F., Rossi, M., Bucci, F., Guzzetti, F. A method for the assessment of the influence of bedding on landslide abundance and types. Landslides 12, 295–309. doi:10.1007/s10346-014-0485-x, 2015b.

Tarchi, D., Casagli, N., Fanti, R., Leva, D. D., Luzi, G., Pasuto, A., Pieraccini, M., Silvano, S.: Landslide monitoring by using ground-based SAR interferometry: an example of application to the Tessina landslide in Italy. Eng. Geol., 68, 1, 15-30, https://doi.org/10.1016/S0013-7952(02)00196-5, 2003.

Teza, G., Galgaro, A., Zaltron, N., Genevois, R.: Terrestrial laser scanner to detect landslide displacement fields: a new approach. Int. J. Remote Sensing, 28, 16, 3425-3446, https://doi.org/10.1080/01431160601024234, 2007.

Torrero, L. Seoli, L. Molino, A. Giordan, D. Manconi, A. Allasia, P. and Baldo, M. The Use of Micro-UAV to Monitor Active Landslide Scenarios, in: Engineering Geology for Society and Territory, edited by: Lollino, G., Manconi, A., Guzzetti, F., Culshaw, M., Bobrowsky P., and Luino, F., Springer International Publishing Switzerland, 5, 701-704, https://doi.org/10.1007/978-3-319-09048-1_136, 2015.

Turner, D.; Lucieer, A. de Jong, S. M.: Time Series Analysis of Landslide Dynamics Using an Unmanned Aerial Vehicle (UAV), Remote Sensing 7(2), 1736-1757, 2015, https://doi.org/10.3390/rs70201736.

Van Den Eeckhaut, M., Poesen, J., Verstraeten, G., Vanacker, V., Nyssen, J., Moeyersons, J., van Beek, L. P. H., and Vandekerckhove, L.: Use of LIDAR-derived images for mapping old landslides under forest, Earth Surf. Proc. Land., 32, 754-769, https://doi.org/10.1002/esp.1417, 2007.

Table 1. Characteristics of the images used to identify and map the Assignano landslide (**Fig. ~~1~~2**). O: order in the sequence of images shown to the interpreter. Platform used to capture the image: W, WorldView-2 satellite; U, UAV. Resolution (ground resolution), in ~~meter~~metre. Spectral (image spectral composite): TCC, True Colour Composite (Red, Green, Blue); FCC, False Colour Composite (Near infrared, Red, Green). Type (image type): M, monoscopic; S, stereoscopic; P, pseudo-stereoscopic. Map: Corresponding landslide map (**Fig. ~~2~~5**).

O	Platform	Resolution	Spectral	Type	Map
1	W	1.~~85~~84	TC	M	C
2	W	1.~~85~~84	FCC	M	D
3	W	1.~~85~~84	TC	S	E
4	W	1.~~85~~84	FCC	S	F
5	U	0.03	TC	M	G
6	U	0.03	TC	P	H

Table 2. Comparison of the total landslide area (A_L), the landslide source and transportation area (A_{LS}), the landslide deposit (A_{LD}), the width and length of the entire landslide (W_L, L_L), of the source and transportation area (W_{LS}, L_{LS}), and of the deposit (W_{LD}, L_{LD}), for eight separate and independent cartographic representations of the Assignano landslide. EL, entire landslide; ST, landslide source and transport area; LD, landside deposit. See **Table 3** for the characteristics of the single maps.

		Map A	Map B	Map C	Map D	Map E	Map F	Map G	Map H
Landslide area (m^2)									
EL	A_L	1.11×10^4	1.91×10^4	1.53×10^4	1.52×10^4	1.09×10^4	1.06×10^4	1.19×10^4	1.16×10^4
ST	A_{LS}	5.40×10^3	7.40×10^3	3.64×10^3	4.02×10^3	5.71×10^3	6.03×10^3	5.21×10^3	5.70×10^3
LD	A_{LD}	5.73×10^3	1.17×10^4	1.16×10^4	1.12×10^4	5.15×10^3	4.59×10^3	6.70×10^3	5.87×10^3
Landslide length (m) and width (m)									
EL	W_L	70.7	97.8	113.4	109.9	61.4	61.25	89.9	85.3
	L_L	362.0	387.5	404.7	391.2	354.6	359.5	343.3	349.1
ST	W_{LS}	51.5	59.6	43.6	49.2	51.92	54.3	49.5	50.5
	L_{LS}	227.9	229.7	205.9	208.0	239.0	239.2	234.7	237.3
LD	W_{LD}	61.0	98.69	111.5	109.0	56.0	57.6	89.9	81.9
	L_{LD}	152.7	172.1	206.2	203.5	129.8	134.7	139	121.8

Table 3. Comparison of the estimated cost, acquisition and pre-processing time, and storage requirement for an area of 4 km^2 (2 km × 2 km) and for an area of 100 km^2 (10 km × 10 km), for monoscopic and stereoscopic satellite images, and for an area of 15 km^2 for photographic images captured by an UAV.

	Satellite monoscopic		Satellite stereoscopic		UAV	
	4 km^2	100 km^2	4 km^2	100 km^2	4 km^2	15 km^2
Acquisition cost (€)	1.500	1.500	3.500	3.500	1.000	3.000
Pre-processing cost (€)	50	50	50	50	250-300	3.000
Acquisition time (day/person)	7-60	7-60	7-60	7-60	1	4
Pre-processing time (hr/person)	1	1	1	1	5-6	20-24
Storage (GB)	0.5	0.5	1	1	12	50
Resolution (m)	2	2	2	2	0.02	0.02
Morphologic signature	no	no	yes	yes	yes	yes
Photographic signature	yes	yes	yes	yes	yes	yes

Figure captions

Figure 1. The Assignano landslide, located near Collazzone, Umbria, central Italy. (A) global view of the landslide. (B) detail of the landslide source area. (C) detail of the landslide transportation area. (D) detail of the landslide deposit. Base image obtained overlaying ("draping") the image on Google Earth™. Red line is the boundary of the landslide obtained using the RTK DGPS (benchmark).

~~**Figure 2**.~~**Figure 2**. Images used to map the Assignano landslide. (A) TC WordView-2 satellite image, (A-I) detail of the source area and (A-II) detail of the landslide deposit. (B) WordView-2 satellite image in FCC, (B-I) detail of the source area and (B-II) detail of the landslide deposit. (C) UAV monoscopic image and C-I a detail of the source area and C-II a detail of the deposition area.

Figure 3. Position of the seven GCPs used to evaluate the co-registration of WordView-2 satellite image (A) and UAV image (B). Corresponding points are illustrated with the same symbol. Differences of the coordinates of the corresponding points along X (i.e., E-W direction, ΔX) and along Y (i.e., N-S direction, ΔY) are provided in metres on the left of the figure.

Figure 4. (A) Overview of the Assignano landslide area in Google Earth™ taken on 8 July 2013. Photo shooting points and photograph taken (B) close to the landslide and (C) from a viewpoint.

The photographs taken in the field and the Google Earth™ image were used to prepare the reconnaissance field map.

Figure 5. Eight independent cartographic representations of the Assignano landslide, "Map A" to "Map H". Map A obtained through a RTK ~~DGPC~~DGPS survey is considered the "benchmark", and shown as a thick black line in the other maps. Map B obtained through reconnaissance field mapping. Map C to Map F obtained through the expert visual interpretation of the satellite images. Map G and Map H obtained through the expert visual interpretation of the orthorectified image taken by the UAV. See **Table 1** for image characteristics. Dark colours show the landslide source and transportation area. Visual inspection of the images reveals the maps most similar to the benchmark.

Figure ~~3. Error matrix obtained from a pairwise comparison of~~ **6**. The error index (*E*) proposed by Carrara et al. (1992), was used to compare quantitatively the different landslide maps ~~prepared for the Assignano landslide, Umbria, Central Italy.~~. (I) Error index matrix for the landslide source and transportation area. (II) Error index matrix for the landslide deposit. (III) Error matrix for the entire landslide. *E* spans the range from 0 (perfect matching) to 1 (complete mismatch).

Figure 47. Comparison of landslide maps prepared for the Assignano landslide, Umbria, Central Italy. (A) Landslide map obtained from a monoscopic (Map C, dark yellow line) and a stereoscopic (Map E, light blue line), true-colour (TC) WordView-2 satellite image (base image), and a mapping of the landslide obtained by walking a GPS receiver along the landslide boundary (Map A, black line). (B) Landslide map obtained from a monoscopic (Map D, yellow line) and a stereoscopic (Map F, cyan line), false-colour-composite (FCC) WordView-2 satellite image, and a mapping obtained by walking a GPS receiver along the landslide boundary (Map A, black line). (C) Landslide map obtained from field survey (Map B, pink line) and from a monoscopic, TC, ultra-resolution image captured by an UAV (Map G, purple line), and the mapping obtained by walking a GPS receiver along the landslide boundary (Map A, black line).

Figure 1

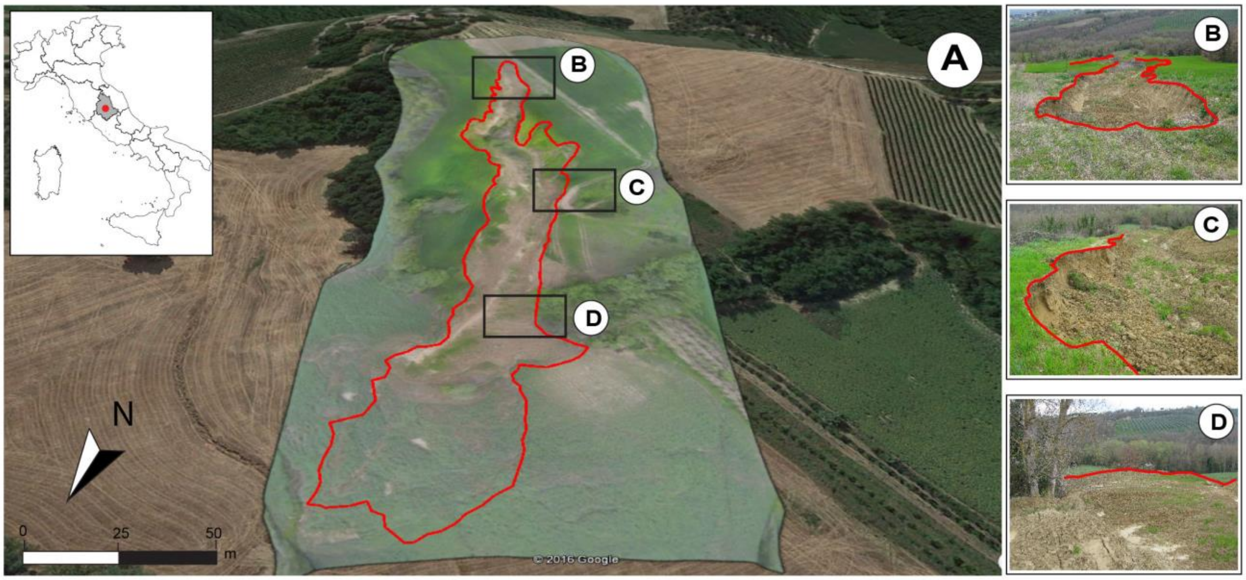

Figure 2

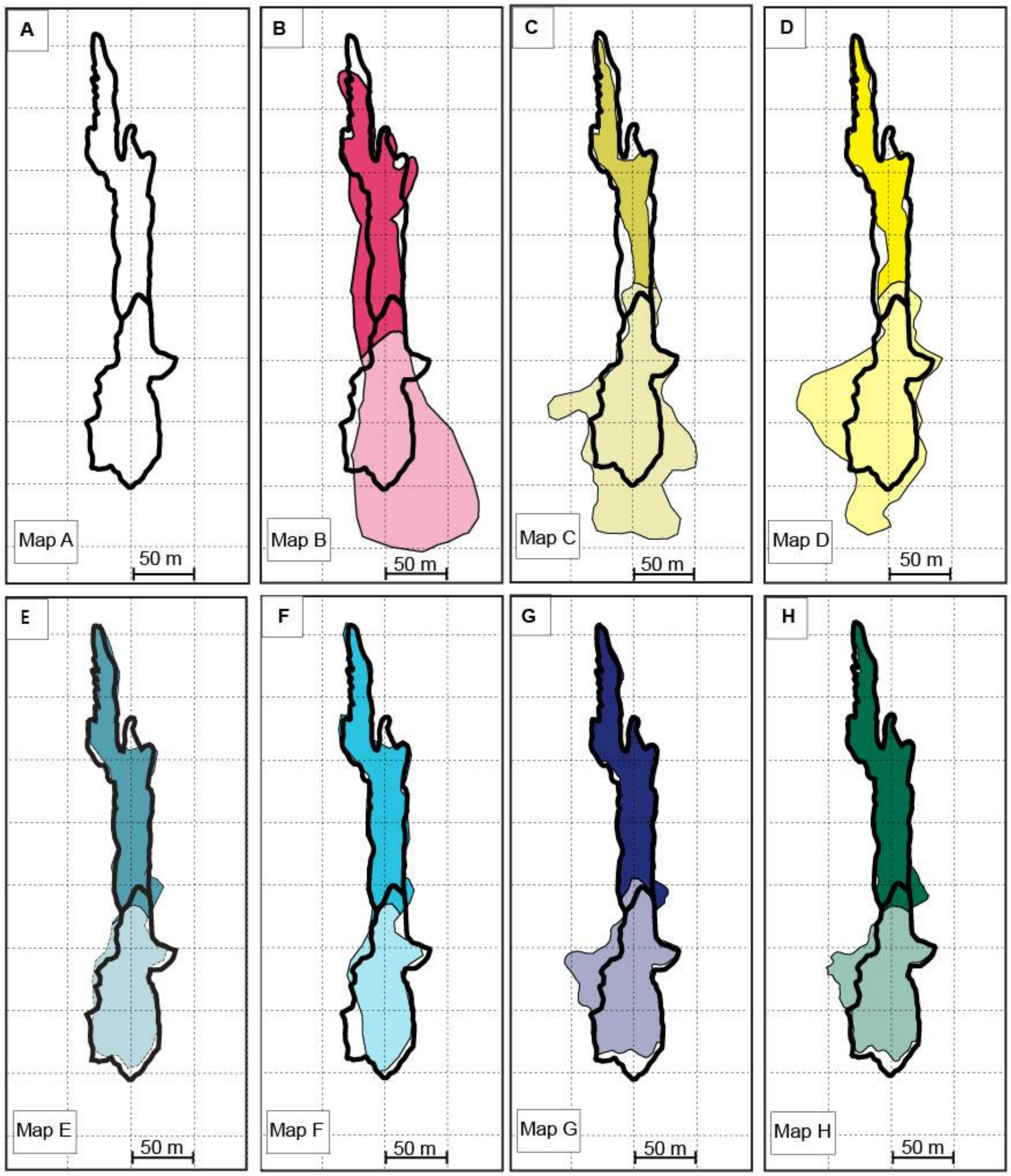
A
Map A
50 m
B
Map B
50 m
C
Map C
50 m
D
Map D
50 m
E
Map E
50 m
F
Map F
50 m
G
Map G
50 m
H
Map H
50 m

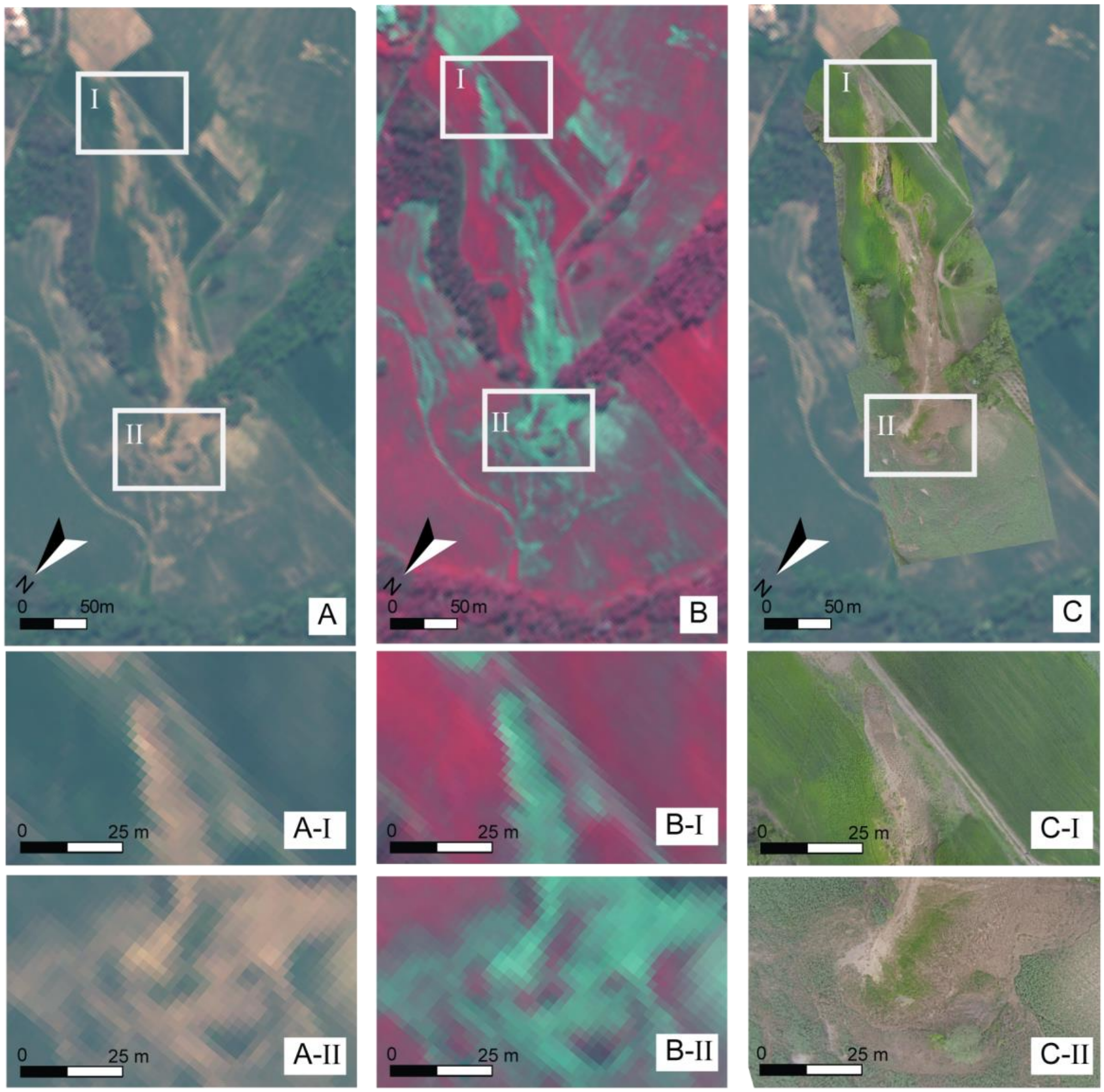

~~Figura~~

Figure 3

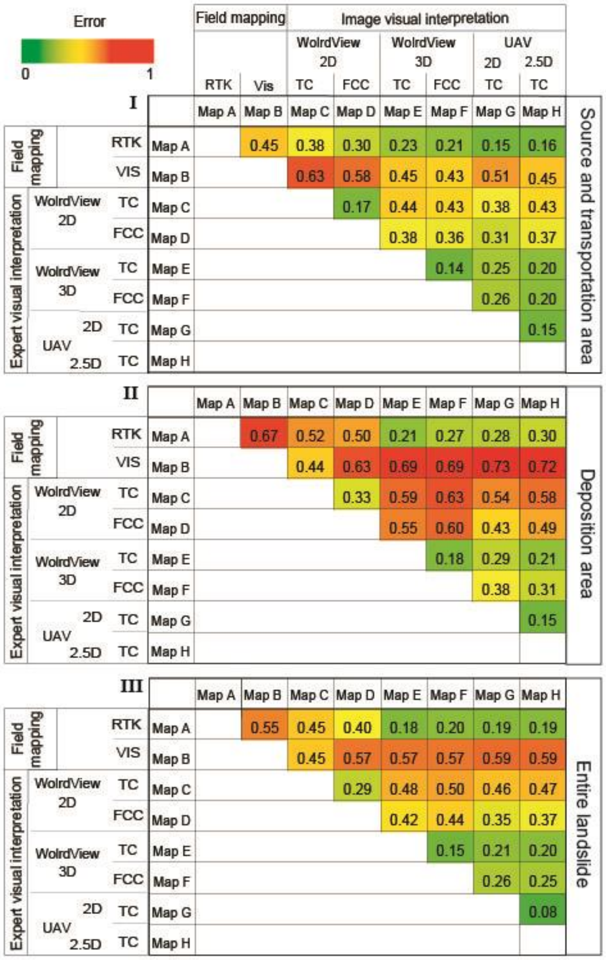

I	Map A	Map B	Map C	Map D	Map E	Map F	Map G	Map H
Field mapping RTK Map A		0.45	0.38	0.30	0.23	0.21	0.15	0.16
Field mapping VIS Map B			0.63	0.58	0.45	0.43	0.51	0.45
WolrdView 2D TC Map C				0.17	0.44	0.43	0.38	0.43
WolrdView 2D FCC Map D					0.38	0.36	0.31	0.37
WolrdView 3D TC Map E						0.14	0.25	0.20
WolrdView 3D FCC Map F							0.26	0.20
UAV 2D TC Map G								0.15
UAV 2.5D TC Map H								

II	Map A	Map B	Map C	Map D	Map E	Map F	Map G	Map H
Field mapping RTK Map A		0.67	0.52	0.50	0.21	0.27	0.28	0.30
Field mapping VIS Map B			0.44	0.63	0.69	0.69	0.73	0.72
WolrdView 2D TC Map C				0.33	0.59	0.63	0.54	0.58
WolrdView 2D FCC Map D					0.55	0.60	0.43	0.49
WolrdView 3D TC Map E						0.18	0.29	0.21
WolrdView 3D FCC Map F							0.38	0.31
UAV 2D TC Map G								0.15
UAV 2.5D TC Map H								

III	Map A	Map B	Map C	Map D	Map E	Map F	Map G	Map H
Field mapping RTK Map A		0.55	0.45	0.40	0.18	0.20	0.19	0.19
Field mapping VIS Map B			0.45	0.57	0.57	0.57	0.59	0.59
WolrdView 2D TC Map C				0.29	0.48	0.50	0.46	0.47
WolrdView 2D FCC Map D					0.42	0.44	0.35	0.37
WolrdView 3D TC Map E						0.15	0.21	0.20
WolrdView 3D FCC Map F							0.26	0.25
UAV 2D TC Map G								0.08
UAV 2.5D TC Map H								

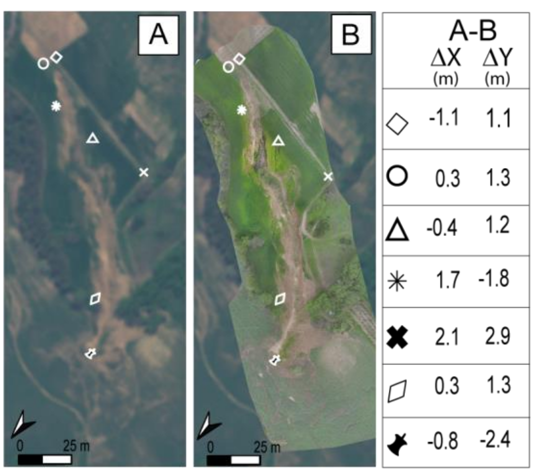

A-B	ΔX (m)	ΔY (m)
◇	-1.1	1.1
○	0.3	1.3
△	-0.4	1.2
✳	1.7	-1.8
✖	2.1	2.9
▱	0.3	1.3
✦	-0.8	-2.4

Figure 4

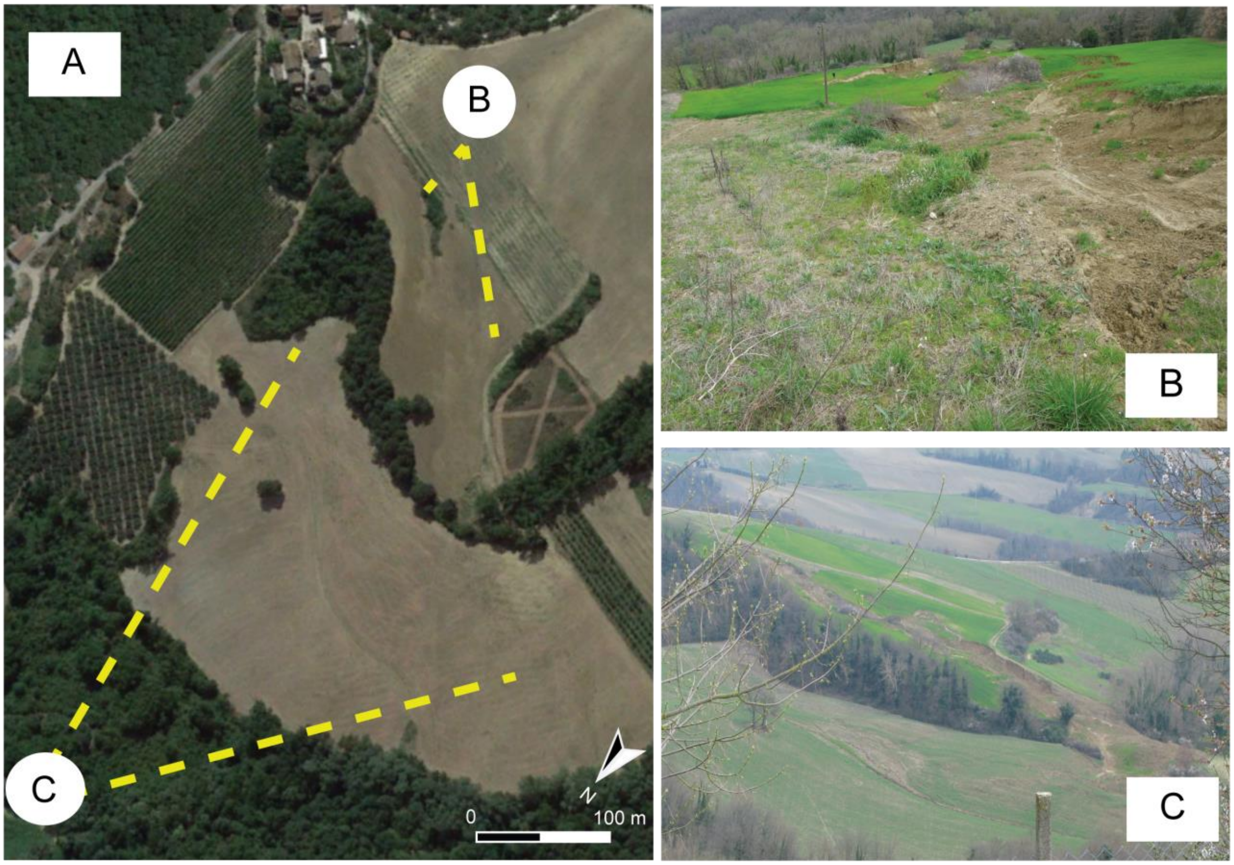

743 **Figure 5**

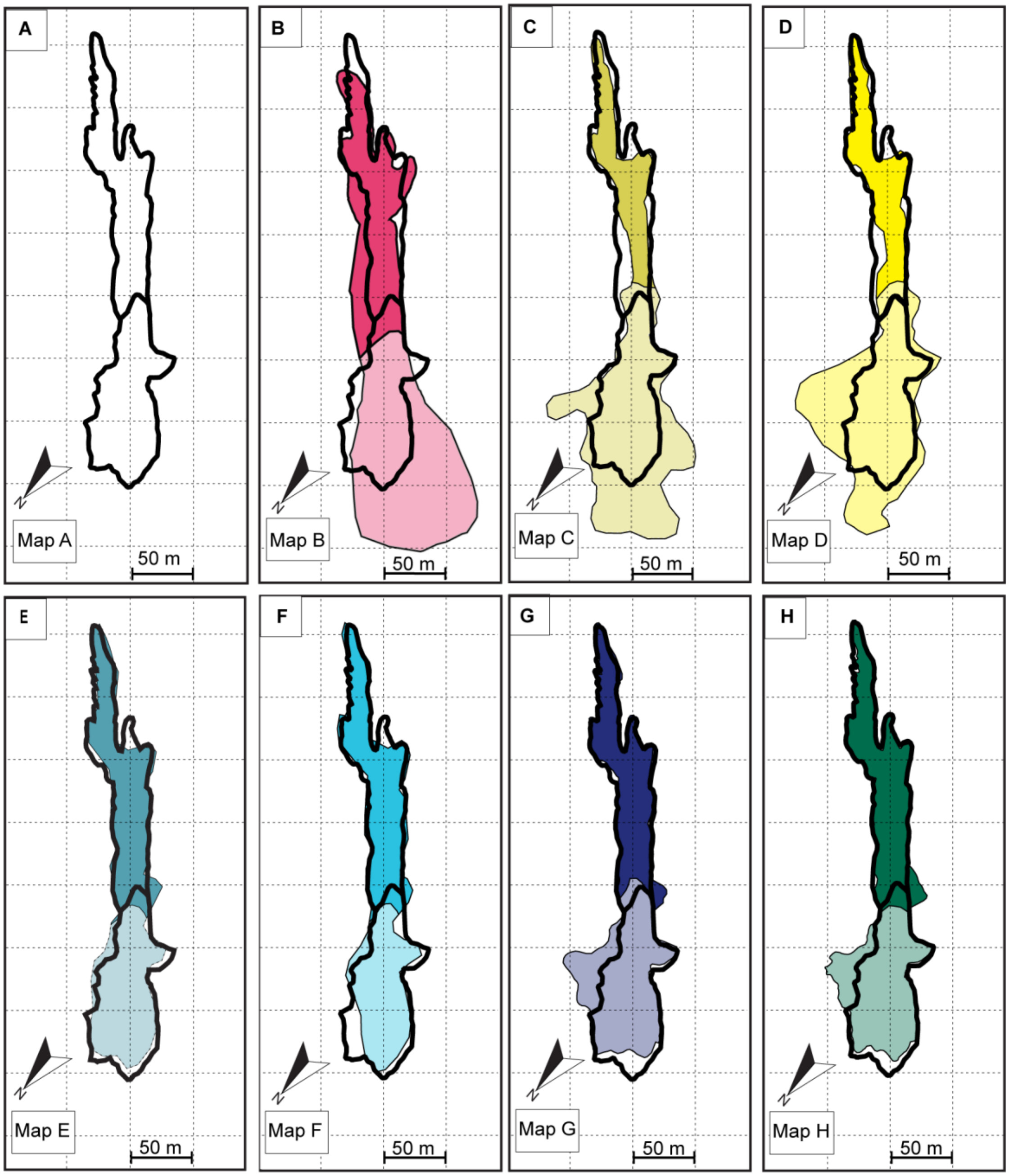

744

Figure 6

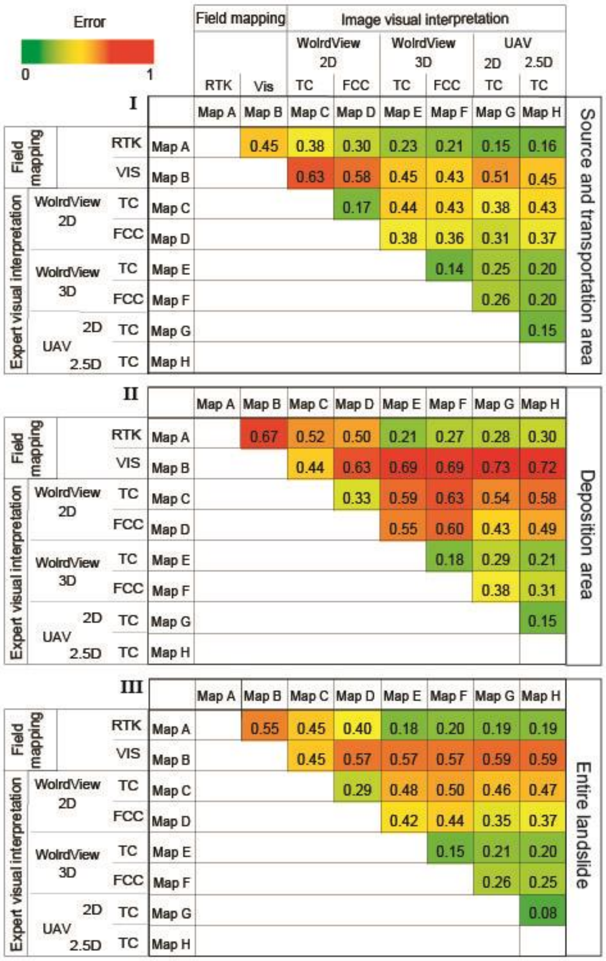
Error
0
1
Field mapping
Image visual interpretation
WolrdView 2D
WolrdView 3D
UAV
2D
2.5D
RTK Vis TC FCC TC FCC TC TC
I
Map A Map B Map C Map D Map E Map F Map G Map H
Field mapping RTK Map A 0.45 0.38 0.30 0.23 0.21 0.15 0.16
VIS Map B 0.63 0.58 0.45 0.43 0.51 0.45
Expert visual interpretation WolrdView 2D TC Map C 0.17 0.44 0.43 0.38 0.43
FCC Map D 0.38 0.36 0.31 0.37
WolrdView 3D TC Map E 0.14 0.25 0.20
FCC Map F 0.26 0.20
UAV 2D TC Map G 0.15
2.5D TC Map H
Source and transportation area
II
Map A Map B Map C Map D Map E Map F Map G Map H
Field mapping RTK Map A 0.67 0.52 0.50 0.21 0.27 0.28 0.30
VIS Map B 0.44 0.63 0.69 0.69 0.73 0.72
Expert visual interpretation WolrdView 2D TC Map C 0.33 0.59 0.63 0.54 0.58
FCC Map D 0.55 0.60 0.43 0.49
WolrdView 3D TC Map E 0.18 0.29 0.21
FCC Map F 0.38 0.31
UAV 2D TC Map G 0.15
2.5D TC Map H
Deposition area
III
Map A Map B Map C Map D Map E Map F Map G Map H
Field mapping RTK Map A 0.55 0.45 0.40 0.18 0.20 0.19 0.19
VIS Map B 0.45 0.57 0.57 0.57 0.59 0.59
Expert visual interpretation WolrdView 2D TC Map C 0.29 0.48 0.50 0.46 0.47
FCC Map D 0.42 0.44 0.35 0.37
WolrdView 3D TC Map E 0.15 0.21 0.20
FCC Map F 0.26 0.25
UAV 2D TC Map G 0.08
2.5D TC Map H
Entire landslide

Figure 7

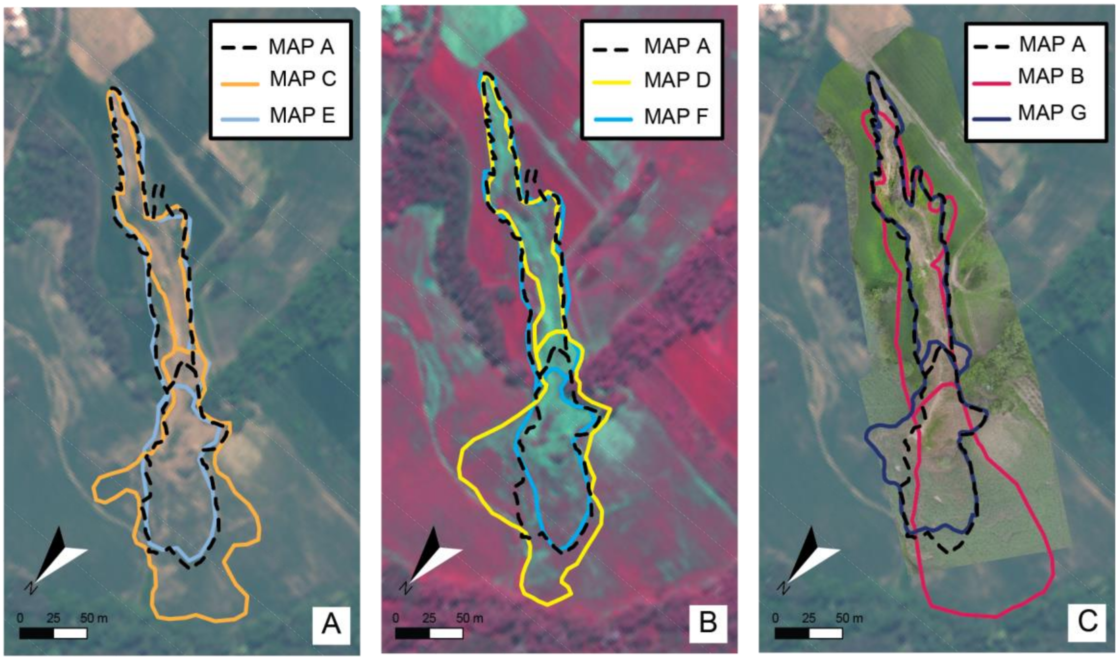
MAP A
MAP C
MAP E
0 25 50 m
A
MAP A
MAP D
MAP F
0 25 50 m
B
MAP A
MAP B
MAP G
0 25 50 m
C